University of Windsor
Scholarship at UWindsor

Electronic Theses and Dissertations | Theses, Dissertations, and Major Papers

1975

Non-linear energy search analysis of truss-type structural systems.

Noor El-Din Mohammed El-Hakim
University of Windsor

Follow this and additional works at: https://scholar.uwindsor.ca/etd

Recommended Citation

El-Hakim, Noor El-Din Mohammed, "Non-linear energy search analysis of truss-type structural systems." (1975). *Electronic Theses and Dissertations*. 2867.
https://scholar.uwindsor.ca/etd/2867

This online database contains the full-text of PhD dissertations and Masters' theses of University of Windsor students from 1954 forward. These documents are made available for personal study and research purposes only, in accordance with the Canadian Copyright Act and the Creative Commons license—CC BY-NC-ND (Attribution, Non-Commercial, No Derivative Works). Under this license, works must always be attributed to the copyright holder (original author), cannot be used for any commercial purposes, and may not be altered. Any other use would require the permission of the copyright holder. Students may inquire about withdrawing their dissertation and/or thesis from this database. For additional inquiries, please contact the repository administrator via email (scholarship@uwindsor.ca) or by telephone at 519-253-3000ext. 3208.

Non-linear energy search analysis of truss-type structural systems
El-Hakim, Noor El-Din Mohammed
ProQuest Dissertations and Theses; 1975; ProQuest

23886

National Library of Canada | Bibliothèque nationale du Canada

CANADIAN THESES ON MICROFICHE | *THÈSES CANADIENNES SUR MICROFICHE*

NAME OF AUTHOR/*NOM DE L'AUTEUR* EL-HAKIM, Noor El-Din Mohamed

TITLE OF THESIS/*TITRE DE LA THÈSE* Non-linear energy search analysis of truss-type structural systems.

UNIVERSITY/*UNIVERSITÉ* University of Windsor, Windsor, Ontario

DEGREE FOR WHICH THESIS WAS PRESENTED/*GRADE POUR LEQUEL CETTE THÈSE FUT PRÉSENTÉE* M.A.Sc.

YEAR THIS DEGREE CONFERRED/*ANNÉE D'OBTENTION DE CE DEGRÉ* 1975

NAME OF SUPERVISOR/*NOM DU DIRECTEUR DE THÈSE* Dr. G. R. Monforton

Permission is hereby granted to the NATIONAL LIBRARY OF CANADA to microfilm this thesis and to lend or sell copies of the film.

The author reserves other publication rights, and neither the thesis nor extensive extracts from it may be printed or otherwise reproduced without the author's written permission.

L'autorisation est, par la présente, accordée à la BIBLIOTHÈQUE NATIONALE DU CANADA de microfilmer cette thèse et de prêter ou de vendre des exemplaires du film.

L'auteur se réserve les autres droits de publication; ni la thèse ni de longs extraits de celle-ci ne doivent être imprimés ou autrement reproduits sans l'autorisation écrite de l'auteur.

DATED/*DATÉ* 6, May 1975 SIGNED/*SIGNÉ* Noor El Din El-Hakim

PERMANENT ADDRESS/*RÉSIDENCE FIXÉ*

NL-91 (11-73)

Reproduced with permission of the copyright owner. Further reproduction prohibited without permission.

NON-LINEAR ENERGY SEARCH ANALYSIS OF TRUSS-TYPE STRUCTURAL SYSTEMS

A THESIS
SUBMITTED TO THE FACULTY OF GRADUATE STUDIES THROUGH
THE DEPARTMENT OF CIVIL ENGINEERING IN PARTIAL
FULFILMENT OF THE REQUIREMENTS FOR THE
DEGREE OF MASTER OF APPLIED SCIENCE
AT THE UNIVERSITY OF WINDSOR

BY

NOOR EL-DIN MOHAMED EL-HAKIM

WINDSOR, ONTARIO, CANADA

1975

Reproduced with permission of the copyright owner. Further reproduction prohibited without permission.

© Noor El-Din Mohamed El-Hakim 1975

557706

Reproduced with permission of the copyright owner. Further reproduction prohibited without permission.

APPROVED BY

[illegible]

J. B. Kennedy

[illegible]

M. C. Temple

Reproduced with permission of the copyright owner. Further reproduction prohibited without permission.

ABSTRACT

The finite element method is applied to the nonlinear analysis of tension and general pin-ended truss-type structures. Geometric and material non-linearities are directly incorporated within the discrete element representation; this permits the prediction of large nodal displacements, yielding of tension members and elastic buckling of individual members.

The principle of minimum total potential energy forms the basis of formulation and solution procedure adopted in this work. Based on the deformed geometry, the total potential energy of a structural system is constructed by summing the energy contributions of the individual elements. Solutions are generated by direct minimization of the total potential energy of the structure in order to find the minimum energy which represents the displacement position at equilibrium. A scaled conjugate gradient unconstrained minimization algorithm is used to locate the minimum of the potential energy. The search procedure automatically detects and considers the effects of slackening of tension members and buckling of compression members.

Reproduced with permission of the copyright owner. Further reproduction prohibited without permission.

Solutions are obtained for a variety of problems to illustrate the potential of the method, and results are compared to those obtained by other solution techniques. The application to prestressed orthogonal and nonorthogonal cable nets and general truss structures, under various loading conditions, have been demonstrated.

Reproduced with permission of the copyright owner. Further reproduction prohibited without permission.

ACKNOWLEDGEMENTS

The writer wishes to express his sincere gratitude to Dr. G.R. Monforton, Professor in charge of this research, for his valuable advice, encouragement and suggestions throughout this study.

The writer is also grateful to the National Research Council for the financial assistant provided during the study period (Grant No. 689).

Thanks are also due to the University of Windsor Computer Center staff.

Reproduced with permission of the copyright owner. Further reproduction prohibited without permission.

LIST OF SYMBOLS

A	cross-sectional area of a truss discrete element.
c,f,g	constants in the theoretical equation for stress-strain curve.
C	generalized displacement coordinate associated with midspan amplitude of the buckling mode in a compression member.
dU	strain energy density.
E	modulus of elasticity.
F	force in truss discrete element.
$\{G_e\}$	gradient vector of the element strain energy.
$\{G\}$	gradient vector of the structure total potential energy.
H	horizontal component of cable tension.
$[H]$	matrix of constants in initial shape determination.
I	bending moment of inertia for compression members.
k_{jj}	element of matrix $[K]$.
$[K]$	matrix of second partials of the total potential energy of the truss structure.
K_1,K_2,K_3	constants of integration appropriate to truss element axial deformation mode.
L	undeformed length of truss discrete element.
n	number of truss discrete elements composing the structure.
N	total number of displacement degrees of freedom of the structure.
p,q	subscripts denoting nodal points of a truss discrete element before deformation.

Reproduced with permission of the copyright owner. Further reproduction prohibited without permission.

$\tilde{p},\tilde{q}$	subscripts denoting nodal points of a truss discrete element after deformation.
$\{P\}$	work equivalent load vector.
$[R]$	diagonal scaling transformation matrix.
$\{S\}$	direction of search in energy minimization.
S	deformed length of truss discrete element.
$\tilde{u},\tilde{v},\tilde{w}$	displacements in the $\tilde{X}$, $\tilde{Y}$ and $\tilde{Z}$ reference coordinate directions, respectively.
u,w	displacements in the x and z local coordinate directions, respectively.
U	strain energy of truss discrete element.
V	volume
W	external work
$\{X\}$	vector of independent degrees of freedom.
$\tilde{X},\tilde{Y},\tilde{Z}$	nodal coordinates in the $\tilde{X},\tilde{Y},\tilde{Z}$ reference coordinate system.
$\{Z\}$	scaled vector of independent degrees of freedom.
ε	strain due to deformation.
ε_p	strain due to prestress.
ε_e	strain at the proportional limit.
σ	stress
σ_p	stress at the proportional limit.
σ_y	the yield stress.
$_p$	total potential energy.

Reproduced with permission of the copyright owner. Further reproduction prohibited without permission.

TABLE OF CONTENTS

Reproduced with permission of the copyright owner. Further reproduction prohibited without permission.

Reproduced with permission of the copyright owner. Further reproduction prohibited without permission.

PAGE

Reproduced with permission of the copyright owner. Further reproduction prohibited without permission.

LIST OF FIGURES

Reproduced with permission of the copyright owner. Further reproduction prohibited without permission.

FIGURE NO. PAGE

Reproduced with permission of the copyright owner. Further reproduction prohibited without permission.

LIST OF TABLES

Reproduced with permission of the copyright owner. Further reproduction prohibited without permission.

CHAPTER I

INTRODUCTION

General truss-type structures, including cable networks, have been recognized as efficient and practical configurations for achieving various structural and architectural objectives. Structural suspension systems are being used with increasing frequency for the support of long-span roofs, providing an unobstructed interior, which makes them suitable for large exhibition halls, stadiums and shopping centers. Also, tension structures are often more economical than conventional structures, since the loads are carried primarily in pure tension; thereby the entire cross-section of the member is utilized to the maximum. The number of compression members is held to the minimum necessary to maintain stability. The economy is achieved in terms of the roof's self-weight where high tensile steel is used in the manufacture of the members.

When a tension or a general truss-type structure deforms considerably under load, the change in geometry complicates the theoretical analysis. Three characteristics common to such structures are responsible for most of the difficulties:

Reproduced with permission of the copyright owner. Further reproduction prohibited without permission.

(1) Geometric nonlinearity (large deflections)

(2) Material nonlinearity (large strains)

(3) Change of configuration (tension members which have no stiffness to compression, may, under certain loading conditions, "go slack")

In order to predict the structural behaviour for such structures, it becomes more realistic to base equilibrium considerations on the deformed geometry, to employ more exact deformation-displacement relations, and to consider the nonlinear behaviour of the material.

It has been found that geometric and material nonlinearities can be conveniently handled by the finite element method, based on the principle of minimum total potential energy. In the finite element analysis, the structure is divided into a number of elements connected at nodes. The deformation state of each element is relatively simple as compared to the deformation state of the whole structure, and is represented in terms of the generalized displacements of the nodes belonging to that element, defined with reference to a fixed global coordinate system. The displacement modes are independent for each element in terms of its generalized nodal displacements. Then the elements are collected together to form the physical structure by satisfying the condition that compatibility of nodal displacements for two or more neighbouring elements ensure displacement

Reproduced with permission of the copyright owner. Further reproduction prohibited without permission.

compatibility at interelement boundaries.

1.1 Literature Survey and Review of Prior Work

During the last decade several studies have been published with different procedures developed for determining the forces and displacements of tension structures and more specifically cable roofs. The early work on this subject was principally focused on the determination of equilibrium shapes.

The finite element method has been used by the majority of research workers in the analysis of tension structures and cable nets. Previous extensions of the finite element displacement method by several authors have treated the problem of geometric nonlinearity with varying degrees of success. Several authors adopted the approach of taking geometric nonlinearity into account by solving a sequence of linear problems. Procedures in this approach are characterized by incremental application of the loading.

A method for the determination of the displacements of a general net was presented by Siev (Ref. 1). The effect of horizontal displacements and changes in geometry were included in the derivation of the equations. An iteration procedure was proposed as a means of solving the equations but no solutions were presented. Siev also suggested incrementing the loads when the problem is highly geometrically nonlinear. The response at each

Reproduced with permission of the copyright owner. Further reproduction prohibited without permission.

stage of the loading is first computed based on a linearizing assumption and then corrected subsequently by iteration. Another paper by Siev (Ref. 2) presented an analytical and experimental study of prestressed suspended roofs bounded by main cables, using the same general theory he had suggested in the previous reference. Thornton and Birnstiel (Ref. 3) derived nonlinear equations for a general three-dimensional unstiffened suspension structure composed of members capable of resisting axial forces only. They presented two numerical methods for the solution of the resulting nonlinear simultaneous algebraic equations, the method of continuity and an incremental load method. Recently, Kumanan (Refs. 4,5) derived equations for a general non-orthogonal cable network with reference to a set of oblique axes to determine the displacements and tensions of the network under load. The derivation is based on the displaced geometry of the structure including second-order displacement terms. The Newton-Raphson method was used for the solution of the resulting nonlinear equations.

Another approach which has been applied successfully to nonlinear analysis of space-type structures is the energy search approach. The energy search approach consists of including geometric nonlinearities by using nonlinear strain-displacement equations to construct the

Reproduced with permission of the copyright owner. Further reproduction prohibited without permission.

potential energy for each of the finite elements. A numerical solution is obtained by seeking the minimum of the total potential energy for the assemblage of finite elements representing the structure. This approach was used successfully by Bogner, Mallet, Minich, and Schmit (Ref. 6); the method has proven to be extremely well suited to the nonlinear analysis as evidenced by the comprehensive problems treated by this method in Ref. 7 which includes instability analysis. The previous work of Ref. 6 was modified by Bogner (Ref. 8) for the application to more general truss-type structures. In Bogner's paper, the governing equations are based on the deformed geometry of the structure; this permits the prediction of large nodal displacements and post-buckled configurations resulting from gross instability of the structure. Bogner used the Fletcher-Powell variable metric search technique (Ref. 9) in the minimization of the total potential energy of the structure. At the same time, Buchholdt (Ref. 10) also developed a theory for prestressed cable-nets based on the minimization of the total potential energy and solved the resulting equations by the method of steepest descent. More recently, Buchholdt (Ref. 11) following the same theory developed in Ref. 10, employed the method of conjugate gradients for the minimization of the total potential energy. He also introduced a scaling technique which increases the

Reproduced with permission of the copyright owner. Further reproduction prohibited without permission.

convergence of the method.

The methods of analysis of the structures reviewed above were based on the assumption of linearly-elastic material behaviour. However, a limited amount of work has been done on these structures stressed into the inelastic region or with nonlinear material properties. Greenberg (Ref. 12) is known as the first to include nonlinear material properties in the analysis of cable roofs. He used a compound curve which is initially linear up to the elastic limit followed by an exponential curve to the ultimate stress. Jonatowski and Birnstiel (Ref. 13) presented a numerical procedure for determining the inelastic behaviour of three-dimensional suspension structures. They used a continuous smooth curve fitted to test results for the cable stress-strain relationship. Like Greenberg, they used a load-increment procedure and determined the ultimate capacity as the load at which the first cable ruptures. Recently, in a dissertation by Kumanan (Ref. 4) the general behaviour of cable networks having hyperbolic paraboloid shapes, orthogonal and non-orthogonal, was studied in the elastic and inelastic regions and their ultimate capacities were determined. Kumanan's theoretical solutions were substantiated by experimental results obtained by testing models of cable networks.

Reproduced with permission of the copyright owner. Further reproduction prohibited without permission.

1.2 Objectives of the Present Study

The following chapters present the systematic development of a finite element capability for predicting the response of truss-type structures (including cable roofs) using the energy search approach.

In Chapter II, the formulations required for the elastic and inelastic analysis of tension members is presented, and includes the prediction of buckling and post-buckling behaviour of truss members capable of resisting compression forces. The total potential energy of an assembly of truss members is employed as the mathematical model. Analytic expressions for the gradient components of the potential energy are generated. The governing equations are based on the deformed geometry of the structure. A straightforward variable correlation scheme which has been thoroughly explained in Ref. 14, is used to impose geometric admissibility between elements.

Chapter III presents the search method used for determining the minimum potential energy position. The conjugate gradient function minimization technique by Fletcher and Reeves (Ref. 15) is discussed. A variable scaling transformation which successfully improves the convergence of the Fletcher-Reeves algorithm is also presented.

Reproduced with permission of the copyright owner. Further reproduction prohibited without permission.

Chapter IV is devoted to numerical evaluations and demonstrates the capabilities of the method of analysis and its effectiveness.

Finally in Chapter V, conclusions are drawn regarding the merit of the approach developed herein for the analysis of general truss and tension structures.

A detailed derivation of the formulation of Chapter II is presented in Appendix A.

A method of determination of the initial shape of a suspension structure is presented in Appendix B.

Reproduced with permission of the copyright owner. Further reproduction prohibited without permission.

CHAPTER II

GENERAL FORMULATION

The discussion in this chapter is focused on presenting the formulation for the potential energy mathematical model of a general truss-type member. Expressions for the strain energy and its analytic gradient are obtained for the member, since both are required for the implementation of the potential energy function minimization technique.

The formulations are based on the deformed geometry of the structure which permits the prediction of large nodal displacements as well as post-buckled configurations; also the inelastic behaviour of tension members is taken into account. Tension members herein are defined as members capable of resisting tension forces only (e.g., cables, ties, and guys); and a general truss member is a member capable of resisting both tension and compression and has pin-ended joints.

The principle assumptions necessary for the mathematical formulations are:

(1) Members are straight and prismatic between joints.

(2) Stressing the members does not change their cross-sectional area.

Reproduced with permission of the copyright owner. Further reproduction prohibited without permission.

(3) Joints of the structure are frictionless.

(4) All loads are conservative, in that their original directions are preserved.

2.1 Elastic Analysis of Tension Members

2.1.1 Deformation-Displacement Relations

The deformation of a general tension discrete element is measured along the x-axis defined by the displaced positions of the element joints $\tilde{p}$ and $\tilde{q}$. A typical tension member in both the undeformed and deformed states is shown in Fig. 1. The undeformed length (L) of a discrete element is defined by the initial positions of the joints p and q (Fig. 1):

$$\bar{L} = \bar{r}_q - \bar{r}_p \qquad (2.1)$$

where $\bar{r}_p$ and $\bar{r}_q$ are the initial position vectors of the element joints prescribed in a common reference coordinate system $(\tilde{X},\tilde{Y},\tilde{Z})$; the undeformed length of an element pq is

$$L = |\bar{r}_q - \bar{r}_p| = \{(\tilde{X}_q-\tilde{X}_p)^2 + (\tilde{Y}_q-\tilde{Y}_p)^2 + (\tilde{Z}_q-\tilde{Z}_p)^2\}^{\frac{1}{2}} \qquad (2.2)$$

Under loading, the joints undergo displacements $(\tilde{u},\tilde{v},\tilde{w})$, measured with respect to the reference coordinate system. The distance between the joints in the deformed position is defined by S:

Reproduced with permission of the copyright owner. Further reproduction prohibited without permission.

$$\bar{S} = (\bar{r}_q + \bar{u}_q) - (\bar{r}_p + \bar{u}_p) \tag{2.3}$$

where $\bar{u}_p$ and $\bar{u}_q$ are the displacement vectors of the element joints; the corresponding deformed length is

$$S = \left\{ [(\tilde{X}_q+\tilde{u}_q) - (\tilde{X}_p+\tilde{u}_p)]^2 + [(\tilde{Y}_q+\tilde{v}_q) - (\tilde{Y}_p+\tilde{v}_p)]^2 + [(\tilde{Z}_q+\tilde{w}_q) - (\tilde{Z}_p+\tilde{w}_p)]^2 \right\}^{\frac{1}{2}} \tag{2.4}$$

2.1.2 Strain-Deformation Relation

The strain of a tension member is expressed in terms of the deformation (u), measured along the deformed length of the member (x-direction). For tension members there is only the axial deformation (u), there is no transverse deformation in the directions perpendicular to the x-axis. Hence, the strain-deformation relation for a tension member is given by

$$\varepsilon = u_x \tag{2.5}$$

This term u_x describes the primary deformation which occurs as the joints of the element displace relative to one another.

2.1.3 Element Strain Energy

The strain energy density is defined by

$$dU = \int_0^{\varepsilon+\varepsilon_p} \sigma \, d\varepsilon \tag{2.6}$$

Reproduced with permission of the copyright owner. Further reproduction prohibited without permission.

Under the assumption of ideal, linear elastic material behaviour,

$$\sigma = E(\varepsilon + \varepsilon_p) \tag{2.7}$$

where ε is the strain of deformation (Eq. 2.5)

ε_p is the strain due to prestress

σ is the stress in the tension member, and

E is the elastic modulus of the material.

Integration of the strain energy density (Eq. 2.6) over the volume (V) of the element results in the following expression for the strain energy in terms of the strain:

$$U = \tfrac{1}{2} \int_V (\varepsilon + \varepsilon_p)\, \sigma \, dV,$$

or

$$U = \frac{E}{2} \int_V (\varepsilon + \varepsilon_p)^2 \, dV \tag{2.8}$$

Substitution for the strain from Eq. 2.5 into Eq. 2.8 and integration over the cross-sectional area (A) yields the strain energy in terms of the local deformation (u) of the element

$$U = \frac{AE}{2} \int_0^S (u_x + \varepsilon_p)^2 \, dx \tag{2.9}$$

where S is the distance between the element joints in the deformed state (Eq. 2.4).

Reproduced with permission of the copyright owner. Further reproduction prohibited without permission.

The governing differential equations for the tension discrete element together with the boundary conditions are derived in Appendix A by taking the first variation of Eq. 2.9.

The governing differential equation is given by

$$\frac{d}{dx}\,(u_x + \varepsilon_p) = 0 \tag{2.10}$$

Integrating Eq. 2.10 gives

$$u_x + \varepsilon_p = K_1 \tag{2.11}$$

where K_1 is a constant with respect to x, and can be determined by integrating Eq. 2.11 over the length S:

$$\int_0^S K_1\, dx = \int_0^S (u_x + \varepsilon_p)\, dx$$

or

$$K_1 = 1 - \frac{L}{S} + \varepsilon_p \tag{2.12}$$

From Fig. 1, the imposed boundary conditions are

$$u\Big|_{x=0} = 0 \quad , \quad u\Big|_{x=S} = S - L \tag{2.13}$$

Reproduced with permission of the copyright owner. Further reproduction prohibited without permission.

It can also be concluded that the force in the member is constant and is given by

$$F = AEK_1 \tag{2.14}$$

The tension element strain energy is obtained in terms of the nodal displacements by substituting Eq. 2.11 into Eq. 2.9 and performing the indicated integration:

$$U = \frac{AE}{2} S K_1^2 \tag{2.15}$$

where S is given by Eq. 2.4, and K by Eq. 2.12. Note that K_1 is directly a nonlinear function of the nodal displacements $(\tilde{u},\tilde{v},\tilde{w})$, measured with respect to the reference coordinate system, through S (Eq. 2.4).

2.1.4 Analytic Gradient of the Element Strain Energy

The gradient of the element strain energy can be defined by the vector $\{G_e\}$ as

Reproduced with permission of the copyright owner. Further reproduction prohibited without permission.

$$\{G_e\} = \begin{Bmatrix} \dfrac{\partial U}{\partial \tilde{u}_p} \\[2ex] \dfrac{\partial U}{\partial \tilde{v}_p} \\[2ex] \dfrac{\partial U}{\partial \tilde{w}_p} \\[2ex] \dfrac{\partial U}{\partial \tilde{u}_q} \\[2ex] \dfrac{\partial U}{\partial \tilde{v}_q} \\[2ex] \dfrac{\partial U}{\partial \tilde{w}_q} \end{Bmatrix} \tag{2.16}$$

where U is the strain energy of the tension element given by Eq. 2.15 given in terms of the nodal displacements of the element $\tilde{u}_p$, $\tilde{v}_p$, $\tilde{w}_p$, $\tilde{u}_q$, $\tilde{v}_q$ and $\tilde{w}_q$. The elements of the gradient vector $\{G_e\}$ are obtained by partial differentiation of the expression for U, with respect to each of the six displacement components of the element; note that both S (given by Eq. 2.4) and K_t (given by Eq. 2.12) are in terms of these six displacement components. This results in the following expressions:

Reproduced with permission of the copyright owner. Further reproduction prohibited without permission.

$$\frac{\partial U}{\partial \tilde{u}_p} = -\frac{AE}{2}\left[(\tilde{X}_q + \tilde{u}_q) - (\tilde{X}_p + \tilde{u}_p)\right] f_1$$

$$\frac{\partial U}{\partial \tilde{v}_p} = -\frac{AE}{2}\left[(\tilde{Y}_q + \tilde{v}_q) - (\tilde{Y}_p + \tilde{v}_p)\right] f_1$$

$$\frac{\partial U}{\partial \tilde{w}_p} = -\frac{AE}{2}\left[(\tilde{Z}_q + \tilde{w}_q) - (\tilde{Z}_p + \tilde{w}_p)\right] f_1 \qquad (2.17)$$

$$\frac{\partial U}{\partial \tilde{u}_q} = -\frac{\partial U}{\partial \tilde{u}_p}$$

$$\frac{\partial U}{\partial \tilde{v}_q} = -\frac{\partial U}{\partial \tilde{v}_p}$$

$$\frac{\partial U}{\partial \tilde{w}_q} = -\frac{\partial U}{\partial \tilde{w}_p}$$

where the term f_1 is given by:

$$f_1 = \frac{K_1^2}{S} + 2K_1\frac{L}{S^2} \qquad (2.18)$$

2.2 Inelastic Analysis of Tension Members

When the stress in a tension member exceeds the material proportional limit, the inelastic range of material behaviour must be considered in deriving the expressions for the element strain energy and its gradient vector.

Reproduced with permission of the copyright owner. Further reproduction prohibited without permission.

2.2.1 Mathematical Model of Stress-Strain Curve

In the analysis of suspension space structures, various mathematical models to represent the stress-strain relationship of the structural element have been adopted by different authors. Greenberg (Ref. 12) used a compound curve which is initially linear up to the elastic limit followed by an exponential curve to the ultimate stress. Jonatowski and Birnstiel (Ref. 13) used a continuous smooth curve fitted to test results. Kumanan (Ref. 4) also used a compound curve which is initially linear up to the proportional limit followed by a second-degree parabola up to the ultimate stress.

The method of analysis presented herein is capable of handling any of these models to represent the inelastic behaviour of tension structures. In the following analysis, the mathematical model presented by Kumanan is adopted to derive expressions for the element strain energy and its gradient vector.

The second-degree parabola between the proportional ~~limit and the~~ point of ultimate stress is assumed to have its axis parallel to the ε (strain) axis as shown in Fig. 2, and is given by the equation

$$\sigma^2 + 2g\varepsilon + 2f\sigma + c = 0 \qquad (2.19)$$

where σ is the stress and g, f, and c are constants

Reproduced with permission of the copyright owner. Further reproduction prohibited without permission.

determined by Kumanan (Ref. 4) as

$$g = -250(\sigma_y - \sigma_p)^2$$

$$f = -\frac{g}{E} - \sigma_p \qquad (2.20)$$

and

$$c = \sigma_p^2$$

where σ_p is the stress at the proportional limit

σ_y is the yield stress, defined as $\sigma_y = (\varepsilon_y - 0.002)E$

and E is the material elastic modulus for the linear part of the curve.

2.2.2 Element Strain Energy

The strain energy density in the inelastic range (Fig. 2) is defined by

$$dU = \tfrac{1}{2}E\varepsilon_e^2 + \int_{\varepsilon_e}^{\varepsilon+\varepsilon_p} \sigma \, d\varepsilon \qquad (2.21)$$

where

$$\sigma = \frac{-2f + \sqrt{4f^2 - 4(2g\varepsilon + c)}}{2}$$

ε is the strain of deformation

ε_p is the strain due to prestress

ε_e is the strain at the proportional limit.

Reproduced with permission of the copyright owner. Further reproduction prohibited without permission.

The strain of deformation is given by

$$\varepsilon = u_x + \tfrac{1}{2} u_x^2 \tag{2.22}$$

where the second order term is considered in order to more accurately account for large strains in the inelastic range.

Proceeding in the derivation of the formulation as has been followed in Section 2.1, the strain energy for a tension member stressed beyond the elastic range of material behaviour is obtained in terms of the nodal displacements (See Appendix A). The resulting element strain energy expression is:

$$U = AS\left[\tfrac{1}{2}E\varepsilon_e^2 + f\varepsilon_e + \frac{1}{24g}(-8g\varepsilon_e + 4f^2 - 4c)^{3/2}\right]$$

$$- ASf(K_2 + \tfrac{1}{2}K_2^2 + \varepsilon_p) - \frac{AS}{24g}\left[-8g(K_2 + \tfrac{1}{2}K_2^2 + \varepsilon_p)\right.$$

$$\left. + 4f^2 - 4c\right]^{3/2} \tag{2.23}$$

where K_2 is a constant given by

$$K_2 = 1 - \frac{L}{S} \tag{2.24}$$

Reproduced with permission of the copyright owner. Further reproduction prohibited without permission.

2.2.3 Analytic Gradient of the Element Strain Energy

Expressions for the elements of the gradient vector $\{G_e\}$ of the element-strain energy are obtained by partial differentiation of the expression for U given by Eq. 2.23, with respect to each of the six displacement components of the element (again noting that both S and K_2 are in terms of these six displacement components):

$$\frac{\partial U}{\partial \tilde{u}_p} = -\frac{A}{S}\left[(\tilde{X}_q + \tilde{u}_q) - (\tilde{X}_p + \tilde{u}_p)\right] f_2$$

$$\frac{\partial U}{\partial \tilde{v}_p} = -\frac{A}{S}\left[(\tilde{Y}_q + \tilde{v}_q) - (\tilde{Y}_p + \tilde{v}_p)\right] f_2$$

$$\frac{\partial U}{\partial \tilde{w}_p} = -\frac{A}{S}\left[(\tilde{Z}_q + \tilde{w}_q) - (\tilde{Z}_p + \tilde{w}_p)\right] f_2 \qquad (2.25)$$

$$\frac{\partial U}{\partial \tilde{u}_q} = -\frac{\partial U}{\partial \tilde{u}_p}$$

$$\frac{\partial U}{\partial \tilde{v}_q} = -\frac{\partial U}{\partial \tilde{v}_p}$$

$$\frac{\partial U}{\partial \tilde{w}_q} = -\frac{\partial U}{\partial \tilde{w}_p}$$

Reproduced with permission of the copyright owner. Further reproduction prohibited without permission.

where the term f_2 is given by

$$f_2 = \tfrac{1}{2}E\varepsilon_e^2 + f\varepsilon_e + \frac{1}{24g}(-8g\varepsilon_e + 4f^2 - 4c)^{3/2}$$

$$- f(K_2 + \tfrac{1}{2}K_2^2 + \varepsilon_p) - f\,\frac{L}{S}(1 + K_2)$$

$$- \frac{1}{24g}\left[-8g(K_2 + \tfrac{1}{2}K_2^2 + \varepsilon_p) + 4f^2 - 4c\right]^{3/2}$$

$$+ \tfrac{1}{2}\,\frac{L}{S}\left[-8g(K_2 + \tfrac{1}{2}K_2^2 + \varepsilon_p) + 4f^2 - 4c\right]^{\frac{1}{2}}(1 + K_2) \qquad (2.26)$$

2.3 Elastic Analysis of Compression Members

In the following, the formulation is extended to the prediction of buckling and post-buckling behaviour of a truss member capable of resisting compression forces. The formulation presented in this section is essentially the same as that presented by Bogner in Ref. 8. A detailed derivation of this formulation is given in Appendix A.

2.3.1 Strain-Deformation Relation

The strain of a compression member is expressed in terms of the deformations (u,w), measured in the local coordinate system (x,z), with origin at the end point $\tilde{p}$ (Fig. 3). The x-axis is defined by the line between the displaced positions of the member joints, the z-axis is normal to the x-axis and lies in the plane of potential buckling. The transverse deformation w, is a secondary

Reproduced with permission of the copyright owner. Further reproduction prohibited without permission.

deformation admitted in the compression member representation in order to provide for buckling of these members within a structural system (local buckling*).

The strain-deformation relation for a general truss member is written in the form

$$\varepsilon = u_x + \tfrac{1}{2}w_x^2 - zw_{xx} \tag{2.27}$$

where z is measured from the neutral axis of the cross-section in the plane of potential bending.

2.3.2 Element Strain Energy

Assuming an ideal linear elastic material, the strain energy of a general truss member is derived in Appendix A. The element strain energy is expressed in terms of the nodal displacements and the buckling amplitude (C) as

$$U = \frac{AE}{2} SK_3^2 + \frac{1}{2}\,\frac{I}{A}\,\frac{\pi^4 C^2}{S^3} \tag{2.28}$$

where S is given by Eq. 2.4, and K_3 is given by

$$K_3 = 1 - \frac{L}{S} + \varepsilon_p + \left(\frac{\pi C}{2S}\right)^2 \tag{2.29}$$

---

*By "local buckling" is meant the buckling of an individual member, while the term "gross buckling" refers to overall instability of the structural system.

Reproduced with permission of the copyright owner. Further reproduction prohibited without permission.

The constant C appearing above is defined as the transverse displacement at midspan of a compression member which is allowed to buckle, and it is retained in the formulation as a generalized coordinate. Note that the value of C remains at zero unless if the member has buckled.

2.3.3 Analytic Gradient of the Element Strain Energy

Expressions for the elements of the gradient vector $\{G_e\}$ of the element strain energy are obtained by partial differentiation of the expression for U given by Eq. 2.28, with respect to each of the six displacement components $\tilde{u}_p$, $\tilde{v}_p$, $\tilde{w}_p$, $\tilde{u}_q$, $\tilde{v}_q$, $\tilde{w}_q$, and, in the case of a buckled member, the midspan displacement C:

Reproduced with permission of the copyright owner. Further reproduction prohibited without permission.

$$\frac{\partial U}{\partial \tilde{u}_p} = -\frac{AE}{2}\left[(\tilde{X}_q + \tilde{u}_q) - (\tilde{X}_p + \tilde{u}_p)\right] f_3$$

$$\frac{\partial U}{\partial \tilde{v}_p} = -\frac{AE}{2}\left[(\tilde{Y}_q + \tilde{v}_q) - (\tilde{Y}_p + \tilde{v}_p)\right] f_3$$

$$\frac{\partial U}{\partial \tilde{w}_p} = -\frac{AE}{2}\left[(\tilde{Z}_q + \tilde{w}_q) - (\tilde{Z}_p + \tilde{w}_p)\right] f_3$$

$$\frac{\partial U}{\partial \tilde{u}_q} = -\frac{\partial U}{\partial \tilde{u}_p} \qquad (2.30)$$

$$\frac{\partial U}{\partial \tilde{v}_q} = -\frac{\partial U}{\partial \tilde{v}_p}$$

$$\frac{\partial U}{\partial \tilde{w}_q} = -\frac{\partial U}{\partial \tilde{w}_p}$$

$$\frac{\partial U}{\partial c} = \frac{AE}{2}\left(\frac{\pi^2 C}{S} K_3 + \frac{I}{A}\frac{\pi^4 C}{S^3}\right)$$

where the term f_3 is given by

$$f_3 = \frac{K_3^2}{S} + 2K_3\frac{L}{S^2} - K_3\frac{\pi^2 C^2}{S^3} - \frac{3}{2}\frac{I}{A}\frac{\pi^4 C^2}{S^5} \qquad (2.31)$$

2.4 Total Potential Energy of a Structural System

The total potential energy of an assembly of n members (tension or general truss members) is defined as

$$\Pi_p = \sum_{i=1}^{n} U^{(i)} - W \qquad (2.32)$$

Reproduced with permission of the copyright owner. Further reproduction prohibited without permission.

where $U^{(i)}$ is the strain energy of the i^{th} element given by either Eq. 2.15, Eq. 2.23, or Eq. 2.28, depending on the type of behaviour the member is following in the assembly, and W is the external work done by the forces applied at the joints of the structure.

In general, the total potential energy of the structural system is a function of N undetermined displacements, which represent the nodal displacements of the structure, measured with respect to the reference coordinate system $(\tilde{X},\tilde{Y},\tilde{Z})$, and the midspan deflections (C) of members permitted to buckle.

Each of the N independent degrees of freedom is assigned a distinct number from 1 to N and a corresponding position in an N-component displacement vector $\{X\}$. The total potential energy of the structural system can then be written as a function of $\{X\}$:

$$\Pi_p(\{X\}) = U(\{X\}) - W(\{X\}) \tag{2.33}$$

where $U(\{X\})$ is the sum of the element strain energies in terms of the independent displacement degrees of freedom $\{X\}$ of the system. The external work done is given by

$$W(\{X\}) = \{X\}^T\{P\} \tag{2.34}$$

where $\{P\}$ is a vector containing the applied loads.

Reproduced with permission of the copyright owner. Further reproduction prohibited without permission.

associated with each of the undetermined displacement degree of freedom in {X}.

2.5 Analytic Gradient of the Total Potential Energy

The conjugate gradient method and its extension by Fletcher and Reeves (Ref. 15) form the basis of an efficient algorithm for solving for the displacements {X} by minimization. It requires only evaluation of the total potential energy of the structural system (Eq. 2.33) and its gradient.

The gradient vector, {G}, of the total potential energy is the vector sum of the gradient vectors of the element strain energies minus the applied load vector {P}. Thus

$$\{G\} = \sum_{i=1}^{n} \{G_e^{(i)}\} - \{P\} \tag{2.35}$$

where the gradient vector $\{G_e^{(i)}\}$ of the i^{th} element is given by either Eq. 2.17, Eq. 2.25, or Eq. 2.30, depending on the type of behaviour the element is following in the assembly. The sum of the gradient vectors of the n elements can be computed by the use of the variable correlation scheme which has been thoroughly explained in Ref. 14.

The necessary condition for the occurrence of a minimum is given by

Reproduced with permission of the copyright owner. Further reproduction prohibited without permission.

$$\{G\} = \{0\}$$

or

$$\frac{\partial \Pi_p(\{X\})}{\partial X_j} = 0 \; ; \; j = 1,2,\ldots,N \tag{2.36}$$

where X_j is the j^{th} component of the vector $\{X\}$.

Reproduced with permission of the copyright owner. Further reproduction prohibited without permission.

CHAPTER III

METHOD OF SOLUTION

The principle of stationary potential energy can be stated as: of all displacement fields {X} which satisfy geometric compatibility, those which locally minimize the potential energy, $\Pi_p(\{X\})$, also satisfy the equilibrium conditions and are stable equilibrium positions. That is:

$$\left.\frac{\partial \Pi_p(\{X\})}{\partial X_j}\right|_{\{X\}=\{X\}^*} = 0 \qquad j=1,2,\ldots,N \tag{3.1}$$

where $\{X\}^*$ is the displacement field at a local minimum. The associated equilibrium position is stable if $\Pi_p(\{X\}^*) < \Pi_p(\{X\})$ for all {X} in some neighbourhood of $\{X\}^*$.

According to the principle of minimum total potential energy, the structural analysis problem can then be viewed as a problem in mathematical programming. The problem is to find the displacement state vector $\{X\}=\{X\}^*$, such that the potential energy function $\Pi_p(\{X\})$ is minimized. The use of mathematical programming methods offers several advantages. First, the potential energy function mathematical model for an individual

Reproduced with permission of the copyright owner. Further reproduction prohibited without permission.

discrete element is significantly simpler to construct than the corresponding direct displacement formulation. The potential energy function mathematical model for the total structure is also constructed with relative ease. The total potential energy is simply the scalar sum of the energy contributions of each element (Eq. 2.32). Secondly, this approach allows the use of powerful numerical methods of mathematical programming to solve the nonlinear structural analysis problem.

The particular type of mathematical programming problem encountered herein is one which the variables X_j are not restricted to certain intervals and is referred to as unconstrained minimization. There is a wide variety of unconstrained minimization methods. Fox (Ref. 16) presented a detailed discussion of these methods and gave valuable guidance in choosing one of them according to the nature of the function to be minimized. The conjugate gradient method and its extension by Fletcher and Reeves (Ref. 15) form the basis of the minimization algorithm used to generate the solutions to the sample problems presented in this work. There are other minimization methods, notably the variable metric method by Fletcher and Powell (Ref. 9); it probably is the most powerful procedure known for finding a local minimum of a general function, and converges reliably, even in ill-conditioned problems,

Reproduced with permission of the copyright owner. Further reproduction prohibited without permission.

but it requires the storage and manipulation of an (N x N) matrix. For the large degrees of freedom systems usually encountered in finite element applications, this procedure involves time consuming matrix operations and storage problems. On the other hand, the Fletcher-Reeves method, although requiring a minimum amount of matrix operations and computer storage, has been characterized by convergence difficulties. Fortunately, the incorporation of a special scaling transformation proposed by Fox and Stanton (Ref. 17) has produced an algorithm which is computationally efficient for the structures included in this study.

3.1 Fletcher-Reeves Unconstrained Minimization Algorithm

The function minimization technique employed in this study is basically described by Fletcher and Reeves in Ref. 15.

The Fletcher-Reeves algorithm begins from an arbitrary initial guess vector, $\{X_o\}$, to the minimum of $\Pi_p(\{X\})$. The initial direction of travel in the N-dimensional space is taken in the negative gradient direction, $\{S_o\}$,

$$\{S_o\} = - \{G_o\} = -\nabla\Pi_p(\{X_o\}) \tag{3.2}$$

Subsequently, the method proceeds by generating directions of descent $\{S_i\}$ $(i = 1,2,\ldots)$ and choosing the step length

Reproduced with permission of the copyright owner. Further reproduction prohibited without permission.

$\alpha_i > 0$ such that $\Pi_p[\{X_i\} + \alpha_i \{S_i\}]$ is a minimum along the direction $\{S_i\}$ at α_i^*. The new approximation to the minimum is achieved at,

$$\{X_{i+1}\} = \{X_i\} \pm \alpha_i^* \{S_i\} \tag{3.3}$$

and subsequent directions are generated from the relations;

$$\{S_{i+1}\} = -\{G_{i+1}\} + \beta_i \{S_i\} \tag{3.4}$$

where

$$\{G_{i+1}\} = \nabla\Pi_p(\{X_{i+1}\}) \tag{3.5}$$

and

$$\beta_i = \frac{\{G_{i+1}\}^T\{G_{i+1}\}}{\{G_i\}^T\{G_i\}} = \frac{|G_{i+1}|^2}{|G_i|^2} \tag{3.6}$$

The Fletcher-Reeves algorithm includes a convergence criterion for accepting α as α^* at which the function value $\Pi_p(\{X\})$ is minimum along the direction $\{S\}$. Note that $\{X\}$ is a vector which minimizes the energy in the previous direction. When the directional derivative $d\Pi_p(\alpha)/d\alpha$ reverses sign, the cubic fit scheme recommended in Ref. 15 is used. The convergence criterion for

Reproduced with permission of the copyright owner. Further reproduction prohibited without permission.

accepting α as α^* was achieved by performing the orthogonality test between {S} and {G} as

$$\frac{\{G\}^T\{S\}}{|G|\ |S|} = \varepsilon_1 \qquad (3.7)$$

where

$$|G| = [\{G\}^T\{G\}]^{\frac{1}{2}} = [\sum_{j=1}^{N} G_j^2]^{\frac{1}{2}}$$

and

$$|S| = [\{S\}^T\{S\}]^{\frac{1}{2}} = [\sum_{j=1}^{N} S_j^2]^{\frac{1}{2}}$$

The quantity ε_1 defined above lies between plus and minus 1 and is zero at α^*. A convergence criterion was also adopted for accepting $\{X\}^*$ as the vector which minimizes the total potential energy function. To accept $\{X\}^*$ as the final solution, the convergence criterion used was

$$\Pi_p(\{X\}^*) - \Pi_p(\{X\}) < \varepsilon_2 \qquad (3.8)$$

which shows that the energy would converge to the minimum according to a specified accuracy ε_2 (a recommended value in the subroutine used is 1×10^{-16}).

Reproduced with permission of the copyright owner. Further reproduction prohibited without permission.

Subroutine DFMC from the IBM System/360 Scientific Subroutine Package was used to find the local minimum of the total potential energy by the Fletcher-Reeves conjugate gradients method.

3.2 Scaling Transformation

Scaling of the variables in the minimization problem is a technique which can materially improve the convergence to the minimum of the function to be minimized.

The term "scaling transformation" as used herein refers to a simple multiplication of the individual degrees of freedom by appropriate constants and thus to a nonsingular diagonal transformation matrix. The objective of scaling, mathematically, is to accomplish a coordinate expansion or contraction which will minimize the "eccentricity" of the function.

For the problems dealt with herein the scaling transformation proposed in Ref. 17 has proven to improve the convergence characteristics and results in an efficient Fletcher-Reeves minimization algorithm. The scaling is based on reducing the ratio of the maximum to the minimum eigenvalues of the matrix of second partials of the function to be minimized. In the case of linearized displacement formulations, the total discretized potential energy can be expressed as

Reproduced with permission of the copyright owner. Further reproduction prohibited without permission.

$$\Pi_p(\{X\}) = \tfrac{1}{2}\{X\}^T[K]\{X\} - \{X\}^T\{P\} \tag{3.9}$$

where $\{X\}$ is the vector of independent degrees of freedom, $\{P\}$ is the work equivalent load vector, and $[K]$ is the ordinary stiffness matrix of the supported structure. In the scaled coordinates this equation will operate as

$$\Pi_p(\{Z\}) = \tfrac{1}{2}\{Z\}^T[\bar{K}]\{Z\} - \{Z\}^T\{\bar{P}\} \tag{3.10}$$

where

$$[\bar{K}] = [R]^{-1}[K][R]^{-1} \;,\; \{\bar{P}\} = [R]^{-1}\{P\} \tag{3.11}$$

The minimization is then carried out with respect to the scaled set of variables

$$\{Z\} = [R]\{X\} \;. \tag{3.12}$$

where $[R]$ is a diagonal matrix with diagonal elements

$$r_{jj} = \frac{1}{(k_{jj})^{\frac{1}{2}}} \qquad j = 1,2,\ldots,N \tag{3.12}$$

In this case, the matrix of second partials of the total potential energy is simply

$$[k] = (k_{ij}) \quad \text{where } i,\ j = 1,2,\ldots,N \;.$$

Reproduced with permission of the copyright owner. Further reproduction prohibited without permission.

In the solution of non-linear problems as those dealt with in the present study, previous experience has proven that a scaling transformation which included the effects of the diagonal elements of the matrices of second partials of the cubic and quadratic terms in the potential energy function does not materially improve convergence. Therefore, in all applications reported herein, the scale factors are obtained from the quadratic terms in the potential energy. The elements of the matrix of second partials are computed from the element stiffness matrices by the use of a variable correlation scheme. Expressions for those terms are derived in Appendix A.

Reproduced with permission of the copyright owner. Further reproduction prohibited without permission.

CHAPTER IV

NUMERICAL EVALUATION AND DISCUSSION OF RESULTS

In this chapter, solutions are obtained for a variety of problems in order to indicate the potential of the present study and to evaluate the approach and method of solution presented herein. The problems examined originate from the published literature which provide a basis for comparison.

A computer program in Fortran IV has been developed for the theoretical analysis of general truss and tension structures with the aid of the IBM 360/50 computer. A minimum of computer storage is required when the energy search approach is adopted since the need for an assembled stiffness matrix (N x N) is eliminated.

The numerical examples examined here includes elastic and inelastic analysis of orthogonal and non-orthogonal prestressed cable nets, and the prediction of response of general truss structures including post-buckling behaviour. The conceptual difficulties associated with tension members dropping out of service (i.e., losing their pretension and becoming slack), or with their yielding (so that the force remains constant in the member when an ideal elastic-perfectly plastic stress-

Reproduced with permission of the copyright owner. Further reproduction prohibited without permission.

strain curve is used), are easily resolved using the energy search approach. The calculation of the total potential energy of a tension structure involves summing the individual contributions from the elements comprising the system (see Eq. 2.32). This provides a natural means to accommodate an altered structural configuration at any point in the search process by simply not including the contribution of slack members in the summation. Provision for buckling or yielding of individual compression members is also included so that gross instability resulting from the accumulation of local effects can be detected. Note that local buckling is considered to occur when the compression force in a truss member exceeds its critical value (Euler Load).

4.1 Numerical Evaluation

4.1.1 Linear Elastic Tension Structures

The results obtained for the tension structures examined below are based on a materially linear elastic behaviour and geometric nonlinearity (formulation of Section 2.1).

EXAMPLE L1:

An orthogonal cable network, having the shape of a hyperbolic paraboloid shown in Fig. 4 was previously analyzed by Thornton and Birnstiel (Ref. 3).

The cross-sectional area of each cable is equal to 1.0 sq. in., the value of the modulus of elasticity is

Reproduced with permission of the copyright owner. Further reproduction prohibited without permission.

equal to 24,000 ksi, and the horizontal component of prestress in all cables is equal to 50 kips. Three cases of loading were considered:

(i) vertical load of 1 kip at each joint,

(ii) vertical load of 1 kip at each joint plus additional load of 14 kips at joint 7,

(iii) in addition to the load in (ii), a horizontal load of 10 kips at joint 7 in the $\tilde{Y}$-direction.

Thornton used the method of continuity for the equilibrium solution of the nonlinear simultaneous algebraic equations, from which the unknown displacement components at the joints could be determined. In the method of continuity, the nonlinear set of simultaneous algebraic equations were transformed into a set of nonlinear differential equations which were integrated.

The results obtained by the present analysis are in very close agreement with those of Thornton's, as seen in Tables 1 and 2.

Using the present analysis, the total potential energy of the structure is a function of 75 degrees of freedom (3 displacement components at each internal node). The search procedure sensed the symmetry of the problem in case (i), although the symmetry of the structure and loading was not taken into consideration in preparing the input data for the computer program.

Reproduced with permission of the copyright owner. Further reproduction prohibited without permission.

It should be mentioned that Thornton has indicated that the geometrically linear and nonlinear solutions for displacements varied by 0.23% for loading condition (i), and by 19% for loading condition (ii). However, the geometrically linear and nonlinear solutions for the horizontal components of cable tensions varied by as much as 101% for loading condition (iii). The non-linearity is more marked in the case of unsymmetrical loading.

By comparing the results, the method of analysis employed here can be said to give accurate results even when the nonlinearity is high (case (iii)).

EXAMPLE L2:

A suspended roof bounded by main cables shown in Fig. 5, was studied analytically and experimentally by Siev in Ref. 2. In Ref. 1 Siev presented a general theory for the determination of the displacements of a general net, taking the horizontal displacements into account. The equations derived were linear and an iterative correction for large deflections using the force imbalance at the joints was suggested.

The model consists of four main cables (1 mm in diameter), 12-13, 13-14, 14-15 and 15-12, fixed at points 12, 13, 14 and 15. Two of the fixing points, 12 and 14, are elevated, and the other two depressed. Four

Reproduced with permission of the copyright owner. Further reproduction prohibited without permission.

diagonals (0.5 mm in diameter) are stretched in each direction between the main cables. The modulus of elasticity was 1.9×10^6 kg/cm^2 for the 0.5 mm diameter wires, and 1.95×10^6 kg/cm^2 for the 1.0 mm diameter wire. The horizontal component (H) of prestress in all diagonal cables was assumed constant and equal to 4.15 kg. The horizontal component (H_1) of prestress in the segments of the main cables was determined from the equilibrium in the horizontal plane (see Appendix C), and is given by the relation,

$$H_1 = 5.65684 \ H$$

All the dimensions, coordinates, and joints elevations are given in Fig. 5. The system is geometrically symmetric about the two diagonal axes.

Siev studied the behaviour of the model under various modes of loading. For comparison, three cases are presented here, for which numerical results are listed in Ref. 2.

In Case (i), the system is loaded at joint "0" with a vertical load incremented from 200 gms to 2000 gms, and the vertical displacement of this joint is provided by both theory and experiment. In the experiment the average of four measured vertical displacements of joints 0, 1, 10 and 11 under the same single vertical load at each of these joints was obtained. The results obtained

Reproduced with permission of the copyright owner. Further reproduction prohibited without permission.

by the present method of analysis together with those by Siev are given in Table 3.

In Cases (ii) and (iii), the system is loaded at all joints with horizontal loads of 0.2 kg and 1.0 kg in the X-direction, respectively. In these cases of loading, there ~~is a~~ symmetry only about the diagonal parallel to the X-axis. Displacements in the X and Z directions of joints 0, 1, 2, 3, 4 and 5 are identical to those of joints 11, 10, 6, 7, 8, and 9 respectively, while displacements ~~in~~ the Y-direction of the same joints are equal in magnitude but opposite in sign. In the present analysis, the potential energy of the structure is a function of 36 degrees of freedom (3 displacement components at each inner joint).

The three displacement components of the joints and the tension for each section for the two cases are compared in Tables 4 and 5.

EXAMPLE L3:

The general behaviour of the orthogonal hyperbolic paraboloid cable-net shown in Fig. 6, was determined by Kumanan in Ref. 4.

The dimensions of the roof in plane are 240 ft. x 120 ft., rising by 12 ft. from A to B, dropping to the same level as A to C, rising again by 12 ft. to D, dropping to the same level as A to E, and finally rising by 12 ft. from E to F. The vertical coordinates of the inner joints are determined using the direct method

Reproduced with permission of the copyright owner. Further reproduction prohibited without permission.

explained in Appendix B, based on the equilibrium of forces at joints.

Values of 24,000 ksi for the elastic modulus, 50 kips for the horizontal components of the pretensioning force for all cables, and 1.25 sq. in. cross-sectional areas for all cables were used.

The structure has 28 inner joints resulting in 84 displacement degrees of freedom. The structure is symmetrical about the line B-E, which therefore reduces the number of displacement degrees of freedom from 84 to 45. The displacement behaviour of the roof was determined under vertical loads of 1.0 kip/joint.

The equations derived by Kumanan to determine the displacements and tensions under load were based on the displaced geometry of the structure, and second order displacement terms were included. The iterative Newton-Raphson method was adapted for the solution of the nonlinear equations.

Typical results of the vertical displacements of the roof joints as given by Kumanan in Ref. 4, together with the results obtained by the present analysis are shown in Table 6.

EXAMPLE L4:

The present method of analysis is efficient and accurate for the study of non-orthogonal cable-roof

Reproduced with permission of the copyright owner. Further reproduction prohibited without permission.

structures. There is no additional provisions to be introduced into the formulation to account for non-orthogonality.

The non-orthogonal hyperbolic paraboloid roof 240 ft. x 120 ft. rising by 12 ft. from A to B, dropping to the same level as A at C, and again rising by 12 ft. to D, as shown in Fig. 7, was analyzed by Kumanan (Ref. 4,5). The vertical coordinates of the inner joints are determined by the method explained in Appendix B.

Values of 24,000 ksi for the elastic modulus, 50 kips for the horizontal components of the pretensioning of all cables, and 1.25 sq. in. for the cross-sectional area of the cables in both directions were used.

The structure has 61 joints involving 183 displacement degrees of freedom, three components at each joint. This number could be reduced to 108 degrees of freedom by considering the antisymmetry about the diagonal AC or DB.

The displacement behaviour of the roof is determined under vertical loads of 1.0 kip/joint, which corresponds to a uniformly distributed load of 5 psf of plan area of the roof.

In Ref. 5, Kumanan derived the equilibrium equations neglecting the higher order terms which is valid only for an infinitesimal load. Two methods to correct

Reproduced with permission of the copyright owner. Further reproduction prohibited without permission.

for nonlinearity when larger loads are applied (an approximate method, and an incremental load method) were used by Kumanan. The approximate method of correction was used to obtain the results for this problem. In this method, half the displacements obtained by solving the equilibrium equations are added to the initial coordinates and the new displacements are calculated using the corrected coordinates. The iteration is continued until the values converge sufficiently. This correction amounts to basing the calculations on a configuration which is half-way between the initial and final (displaced) configurations.

Typical results of the vertical displacements of the roof joints as given by Kumanan in Ref. 5, together with the results obtained by the present analysis are shown in Table 7.

4.1.2 Inelastic Tension Structures

The inelastic analysis and the determination of the ultimate load capacity of the two cable-net roofs previously analyzed (EXAMPLES L3 and L4) were carried out considering material nonlinearity. The same theoretical model for the stress-strain curve suggested by Kumanan (Ref. 4) is adapted here for developing the energy search approach to include the study of inelastic behaviour of cable roofs under increasing load (see Chapter II, Section 2.2).

Reproduced with permission of the copyright owner. Further reproduction prohibited without permission.

In the numerical calculations of the ultimate load, values of 24,000 ksi for the elastic modulus, 124.9 ksi for the proportional limit, 155 ksi for the yield stress, 250 ksi for the ultimate stress, and 4.5% for the ultimate strain were used. Accordingly, the stress-strain curve relationship (Eq. 2.19) is given by

$$\sigma^2 - 453000\ \varepsilon - 230.925\ \sigma + 15600 = 0$$

where σ is the stress in ksi and ε is the strain.

The criterion of failure of the roof is defined as when the ultimate stress is reached in the most highly stressed segment of the cables. Kumanan used an incremental load method where the tangent modulii corresponding to the stress levels in the cables were used throughout the derived equations. The external applied load was incrementally increased until the ultimate load was reached.

The value of the ultimate load for the orthogonal cable-net obtained by Kumanan was 65.2 kips/joint with a maximum deflection of 15.9 ft., while for the non-orthogonal cable-net the ultimate load was 49.1 kips/joint with a maximum deflection of 22.5 ft.

By the present energy search approach, the value of the ultimate load for the orthoginal cable-net was calculated and found to be 67.7 kips/joint, with a

Reproduced with permission of the copyright owner. Further reproduction prohibited without permission.

maximum deflection of 15.6 ft., and for the non-orthogonal cable-net the ultimate load was 49.2 kips/joint with a maximum deflection of 22.8 ft. In generating the ultimate load, the external applied load was increased by 4 kips/joint, starting from initial load of 4 kips/joint, and a smaller increment (0.1 kips/joint) was used to arrive at the final value of the ultimate load. It should be mentioned that no provisions were made in the formulations to account for the occurrence of unloading of cable segments. The load-stress history of the roof's cable segments indicated no case of cable unloading in the inelastic range.

4.1.3 Linear Elastic General Truss Structures

EXAMPLE G1:

The truss structure investigated below, together with the applied loading is completely described in Fig. 8. It is essentially the same structure investigated in Ref. 6 (Case T2).

The formulation presented in the present work for compression members is essentially the same as that developed in Ref. 6, except for the three refinements suggested by Bogner in Ref. 8:

(1) the possibility of including prestress,

(2) the assumed transverse displacement state is assumed to be proportional to the first buckling eigenmode instead of a polynomial, and

Reproduced with permission of the copyright owner. Further reproduction prohibited without permission.

(3) the capability of handling change of configuration is provided.

This example is intended to indicate the applicability of the geometrically nonlinear truss finite elements presented to the prediction of finite displacements and post-buckling behaviour. The force and displacement behaviour predicted by three different mathematical models of the structure are presented as obtained in Ref. 6, together with the results obtained by the present analysis in Tables 8 and 9, respectively.

The results shown in column 2 of Tables 8 and 9, were predicted by a conventional linear matrix method. In columns 3 and 4 of the table, the behaviour predicted assuming large displacements of the nodes but no buckling, is presented. Finally, the prediction of large node displacements and post-buckling configuration, is presented in columns 5 and 6.

The results obtain by the present analysis are basically the same as Ref. 6, as can be seen in the two tables. The slight differences seen between the two results is attributed to:

(1) In Ref. 6, the buckled shape of a truss compression element is approximated by an assumed polynomial with five coefficients determined from the imposed and natural boundary conditions. In the present work, the assumed transverse displacement of a truss

Reproduced with permission of the copyright owner. Further reproduction prohibited without permission.

compression element is taken to be proportional to the first buckling eigenmode (Eq. A-42) which precisely represents the buckling shape.

(2) The prediction of the behaviour of the truss with the simultaneous consideration of large nodal displacements and local buckling was based on the stiffness characteristics of the individual discrete elements. The stiffness characteristics of the truss compression element in its two deformed states, straight and buckled, was evaluated in Ref. 6. The critical load for the truss element was estimated to be 0.2% greater than the Euler buckling load. This explains the slight difference in the results in columns 5 and 6 of the tables. In the present analysis, the critical load for the truss element is exactly taken to be equal to the Euler buckling load (Eq. A-40).

Provision for local buckling detection is easily incorporated in the computer program. Local buckling of individual members occurs when the force in a truss member exceeds its critical value (Euler load). Simply, the value of the variable K_3 given by Eq. A-43, is investigated during the search process. If the value of K_3 was found to be negative, and it is greater than or equal to K_{3cr} given by Eq. A-39, then the value of K_3 is set equal to K_{3cr}, i.e., the force in the truss member is set exactly equal to the buckling load.

Reproduced with permission of the copyright owner. Further reproduction prohibited without permission.

In the case of the prediction of the truss behaviour assuming large nodal displacements but not allowing buckling, the potential energy of the structure was a function of 6 degrees of freedom, namely the displacements of nodes 5 and 6. For the case assuming large nodal displacements and where four truss members are permitted to buckle, the potential energy was a function of 10 degrees of freedom, 6 nodal displacements at nodes 5 and 6, plus 4 midspan displacements (describing the local transverse displacement state of the members which are permitted to buckle, Eq. A-42). The four truss members (1-5), (2-6), (3-5), and (4-6) were permitted to buckle on the basis of the behaviour results predicted by the linear method.

It should be emphasized that the error inherent in the behaviour predicted linearly is apparent. It is also clear that local buckling influences the force distribution more than the nodal displacements.

EXAMPLE G2:

As a final example, the suspended dome-truss structure shown in Figures 9 and 10 is studied. The structure consists of a 120 ft. diameter shallow truss dome 6 ft. in height (Fig. 9). The dome has 42 tubular aluminum members (round tube section of diameter = 4½ in., A = 1.718 in.^{2}, I = 4.114 in.^{4}, and

Reproduced with permission of the copyright owner. Further reproduction prohibited without permission.

weight of 2.02 pounds per ft.). The shallow dome is suspended from the nodes on the outer circumference by 12 slender hangers (each 12 ft. long, A = 0.1 in.^{2}) to a horizontal network of orthogonal prestressed cables (Fig. 10). The prestressed cable network (high tensile steel wires, A = 0.5 in.^{2}) provides the strength necessary to support the loads involved in the analysis. The prestress force in each cable of the network is taken equal to 25 kips.

The behaviour of this structural system demonstrates the effectiveness of the analysis and permits the investigation of a snap-through phenomenon as well as the post-buckling behaviour coupled with the response of a typical cable network.

The total potential energy of the structure is a function of 162 degrees of freedom (120 nodal displacement components of the structure's 40 nodes, plus 42 possible midspan buckling amplitudes of the dome bars); symmetry was not taken into consideration, however, complete symmetry in displacements and stresses resulted in all loading conditions. In the following discussion, load-displacement histories are generated and the search procedure uses the solution for the previous loading condition as the starting point for the current loading condition. For gradual load incrementation this feature is a somewhat helpful as a computer time-saving device;

Reproduced with permission of the copyright owner. Further reproduction prohibited without permission.

however, solutions are obtained essentially independently for each loading case, since the method of solution itself is not a load incrementation scheme.

Two cases of behaviour response are studied:

Case (i): The dome is suspended only from the circumference joints. Initially the dead weight of the structure is considered as concentrated loads at all the dome joints; then an external downward load at joint 1 is superimposed in 100 lbs. increments.

The load-displacement histories for nodes 1 and 2 are shown in Figures 11 and 12, while the load-force histories of members A, C, D and E are shown in Fig. 13. Inspection of the figures indicate that the relationships are linear up to a superimposed load at node 1 of 610 lbs. At this load members A and B buckle and is accompanied by a "snap-through" buckling phenomenon of the complete dome structure resulting in a configuration which is inverted with respect to the original configuration. The large displacements that result are shown in Figures 11 and 12 where it is seen that node 1 snaps from a "small" deflection of 0.9248 ft. to a large deflection of 12.89 ft. and node 2 from 0.7836 ft. to 9.78 ft.

Inspection of Fig. 13 reveals that all the dome members which were in tension prior to the "snap-through" become compression members and all dome members

Reproduced with permission of the copyright owner. Further reproduction prohibited without permission.

which were compression members become tension members (including members A and B).

As the load increased from 610 lbs., the behaviour is again linear as indicated in Figs. 11, 12 and 13. At a load of 1240 lbs. the outer circumferential members (D) buckle. The buckling of members D again cause a change in the shape of the load-deflection histories as the load is increased beyond 1240 lbs. (Figs. 11 and 12). Once that members D have buckled the forces in members D remains constant (Fig. 13) and the tension force in member E also remains constant in agreement with equilibrium considerations. The forces in members A follow a linear relationship from the snap-through buckling load of 610 lbs. until a load of 1870 lbs. is reached at which members C also buckle. Although the structural behaviour could have been monitored further, it was felt that the effectiveness of the analysis procedure had been demonstrated and that a practical alternative involved preventing the snap-through buckling phenomenon as described in the following discussion.

Case (ii): In addition to the 12 hangers of case (i), three more hangers (A = D.1 in.^{2}) are introduced between nodes 1, 2 and 12 of the dome and nodes 20, 21 and 25 of the cable network, respectively.

Reproduced with permission of the copyright owner. Further reproduction prohibited without permission.

Starting from the dead weight loads of the dome and superimposing loads at node 1 the behaviour is predicted.

The load-displacement histories for nodes 1, 2, 4 and 5 are shown in Fig. 14, while the load-force histories for members A, B, C and for the hangers at nodes 1, 2 and 3 are shown in Figures 15 and 16, respectively. In all cases, the relationships are basically linear until the superimposed load at node 1 reaches 1160 lbs. At this load, members A and B buckle and the hangers at nodes 2 and 12 go slack. Therefore, any increase in load at node 1 causes a redistribution of forces in the non-buckled members, since the buckled members cannot carry any additional load and also since the hangers at nodes 2 and 12 cannot take any compression forces. It is therefore seen in Fig. 14 that the deflection of node 1 increases more rapidly as the load is increased beyond the load which causes buckling in members A and B. This is accompanied by a more rapid increase of the force in the hanger at node 1 and a decrease of the forces in the circumferential hangers as shown in Fig. 16. Since the hanger at node 1 resists a higher percentage of the superimposed load after buckling, less load is carried by the truss members as exemplified by the load-force history of member C (Fig. 15). The load-deflection behaviour of nodes 2 and 4 after buckling (Fig. 14) is a result of

Reproduced with permission of the copyright owner. Further reproduction prohibited without permission.

the combined effect of buckling of the six truss members, the change of force levels in the hangers, the slackening of the hangers of node 2 and 12 and the change of geometry of the suspended structure.

Note that the additional hangers preclude the possibility of a snap-through buckling phenomenon.

Reproduced with permission of the copyright owner. Further reproduction prohibited without permission.

CHAPTER V

SUMMARY AND CONCLUSIONS

The finite element method has been applied to the nonlinear analysis of general truss-type structures. Geometric nonlinearity was incorporated in the analysis by using nonlinear deformation-displacement and strain-displacement relations. The governing equations are therefore based on the deformed geometry of the structure which permits the prediction of large nodal displacements and post-buckled configurations; the formulation also allows the detection of general instabilities which result from the occurrence of unstable deformed nodal configuration due to the accumulation of local instabilities. In the case of tension members, the analysis presented also incorporates material nonlinearities (i.e., nonlinear stress-strain relationship).

The method presented does not require the use of a load incrementation procedure followed by many researchers to deal with nonlinear structural problems; load incrementation is avoided herein by direct incorporation of the nonlinearities into the formulation.

Reproduced with permission of the copyright owner. Further reproduction prohibited without permission.

The method of analysis developed herein represents an advance toward more realistic prediction of the behaviour of general truss-type structures.

The potential energy function mathematical model of a structural system of finite elements presented in this work is generally simpler to construct than the corresponding direct displacement formulation. The calculation of the total potential energy of the structure is simply the scalar sum of the energy contributions from the individual members which comprise the structure; the construction of the direct displacement formulation would require the additional effort of either taking the variation of the potential energy or considering equilibrium explicitly at each node point with reference to the deformed position (Refs. 1, 3, 4, 5). The potential energy function mathematical model for an individual discrete element is also constructed with relative ease.

The direct search for the position of the minimum total potential energy function of the structure using the Fletcher-Reeves unconstrained minimization algorithm incorporated with a variable scaling transformation was found to be efficient and gives accurate solution for nonlinear problems. No convergence problems were encountered; solutions were obtained for every problem within a reasonable number of iterations.

Reproduced with permission of the copyright owner. Further reproduction prohibited without permission.

The energy search approach has proven to provide a natural means to accommodate changes in structural configuration due to slackening of tension members and buckling of compression members. The method also was capable of dealing with yielding of tension members (material nonlinearity), and the determination of the ultimate load capacity of cable roofs. The accuracy of the method appears acceptable for all the cases investigated in the previous chapter where comparisons with results by other different approaches were made.

Finally, the formulation presented can serve as a basis to derive similar formulations for structural members with other than pin-connected ends; this would permit the analysis of stayed and guyed towers which are a combination of tension members and stringer-column members.

The previous discussion can be summarized by the ensuing conclusions which pertain to the following nonlinear structural analysis problems dealt with herein:

(a) Prestressed orthogonal and nonorthogonal cable nets (including large nodal displacements, slackening of cable segments and material nonlinearity).

(b) General truss-type structures (including large nodal displacements, slackening of tension members, buckling of individual compression members, prediction of gross buckling loads and post-buckling behaviour).

Reproduced with permission of the copyright owner. Further reproduction prohibited without permission.

1. The energy search formulation presented is an efficient alternative to direct formulation methods with respect to the total effort required to formulate and solve the above nonlinear structural analysis problems.
2. The Fletcher-Reeves algorithm used for the minimization of the total potential energy of the structure is an efficient tool for the analysis of tension and general truss structures.
3. The method presented handles the difficulties associated with the behaviour of tension and general truss structures efficiently and accurately.

Reproduced with permission of the copyright owner. Further reproduction prohibited without permission.

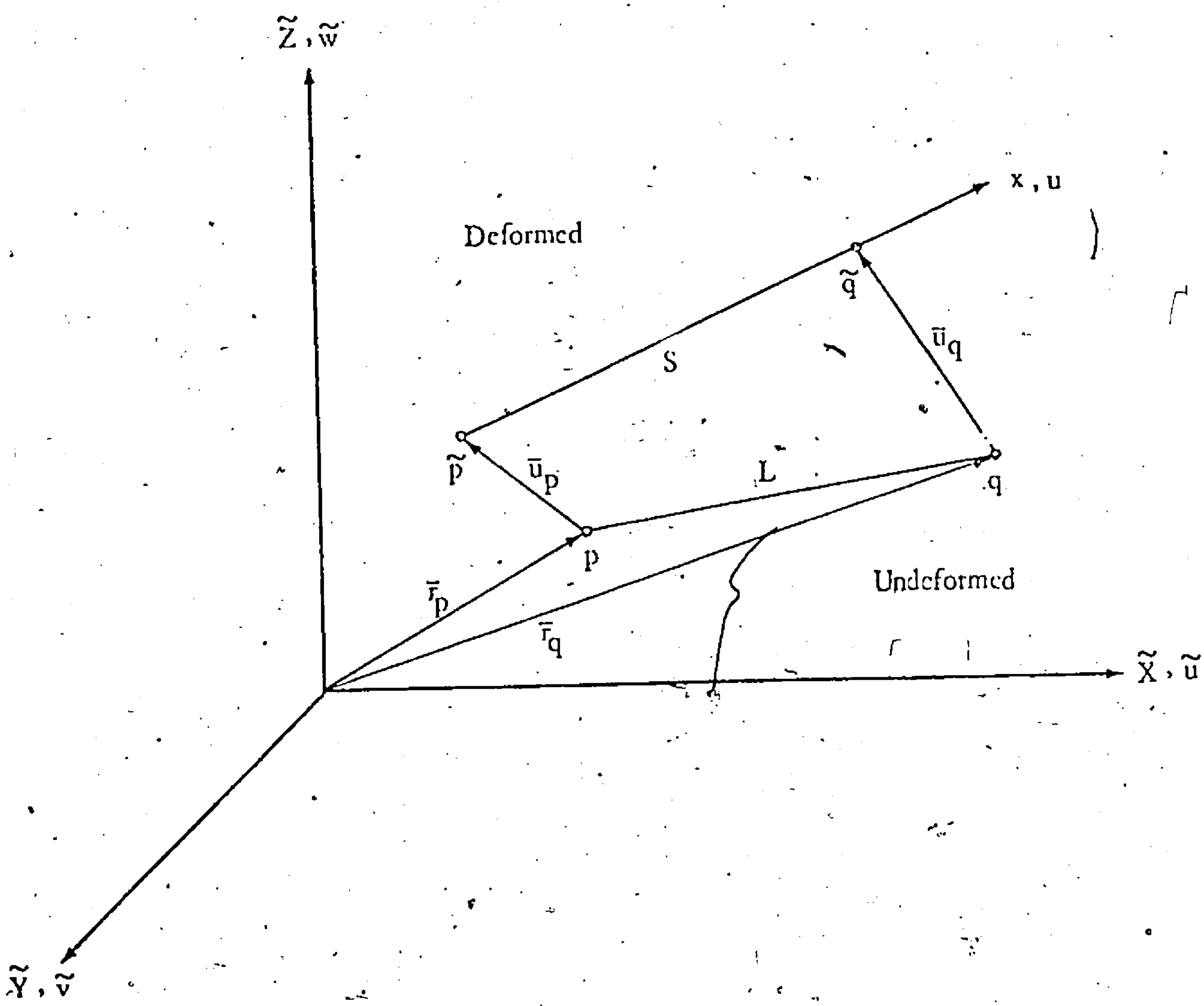

Figure 1. Tension Discrete Element.

Reproduced with permission of the copyright owner. Further reproduction prohibited without permission.

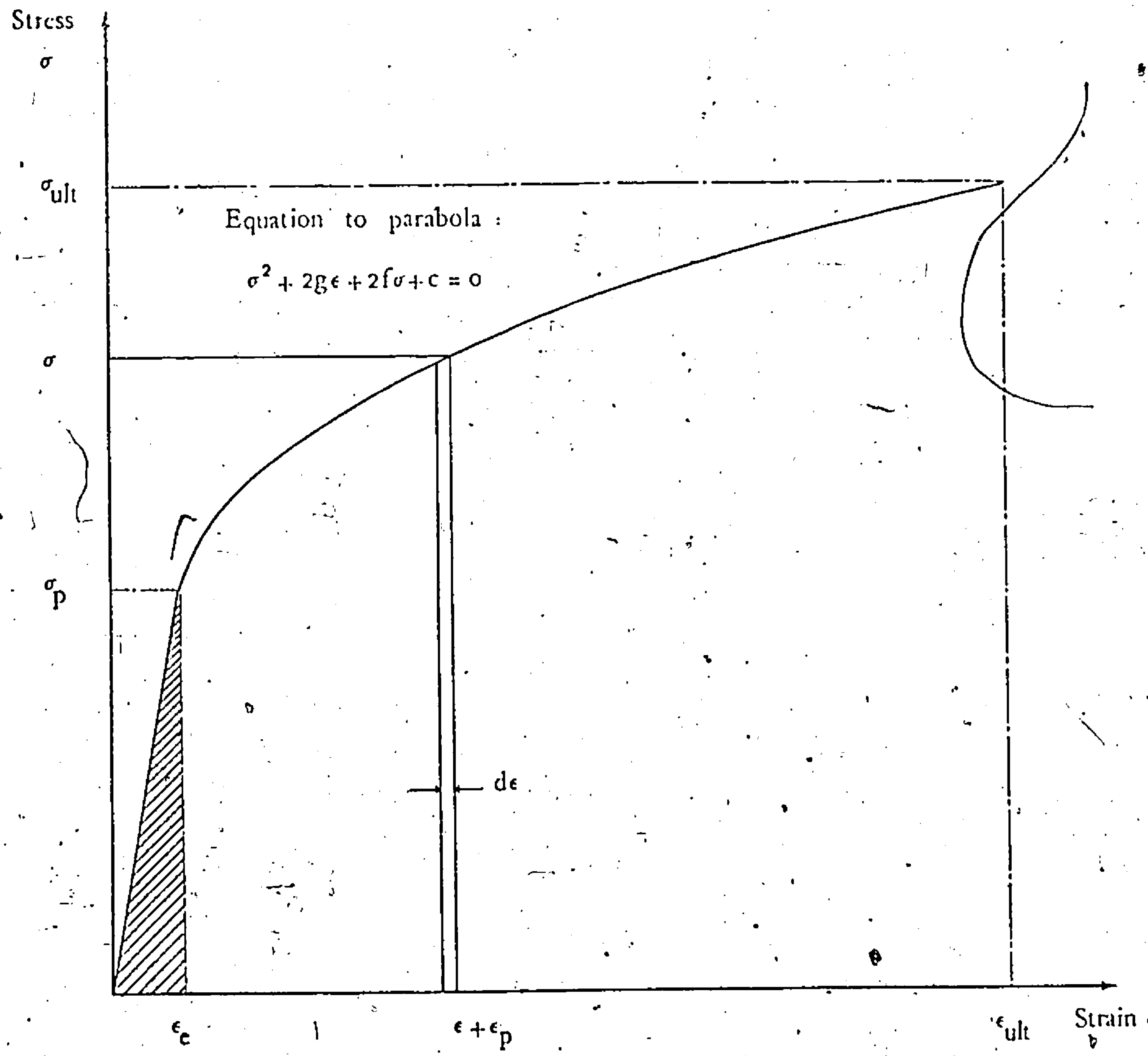

Figure 2. Stress-Strain Curve for Cable.

Reproduced with permission of the copyright owner. Further reproduction prohibited without permission.

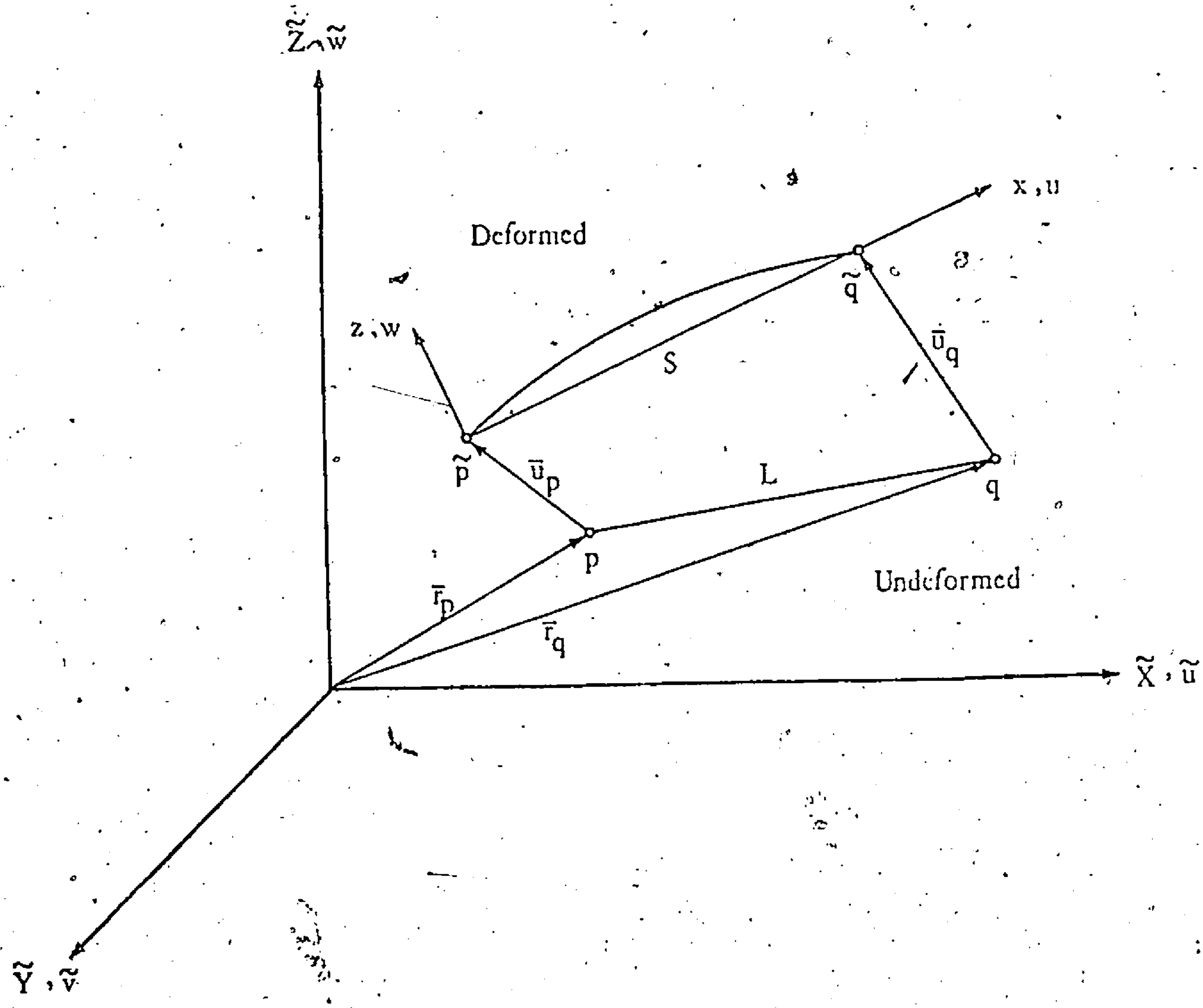

Figure 3. Compression Truss Discrete Element.

Reproduced with permission of the copyright owner. Further reproduction prohibited without permission.

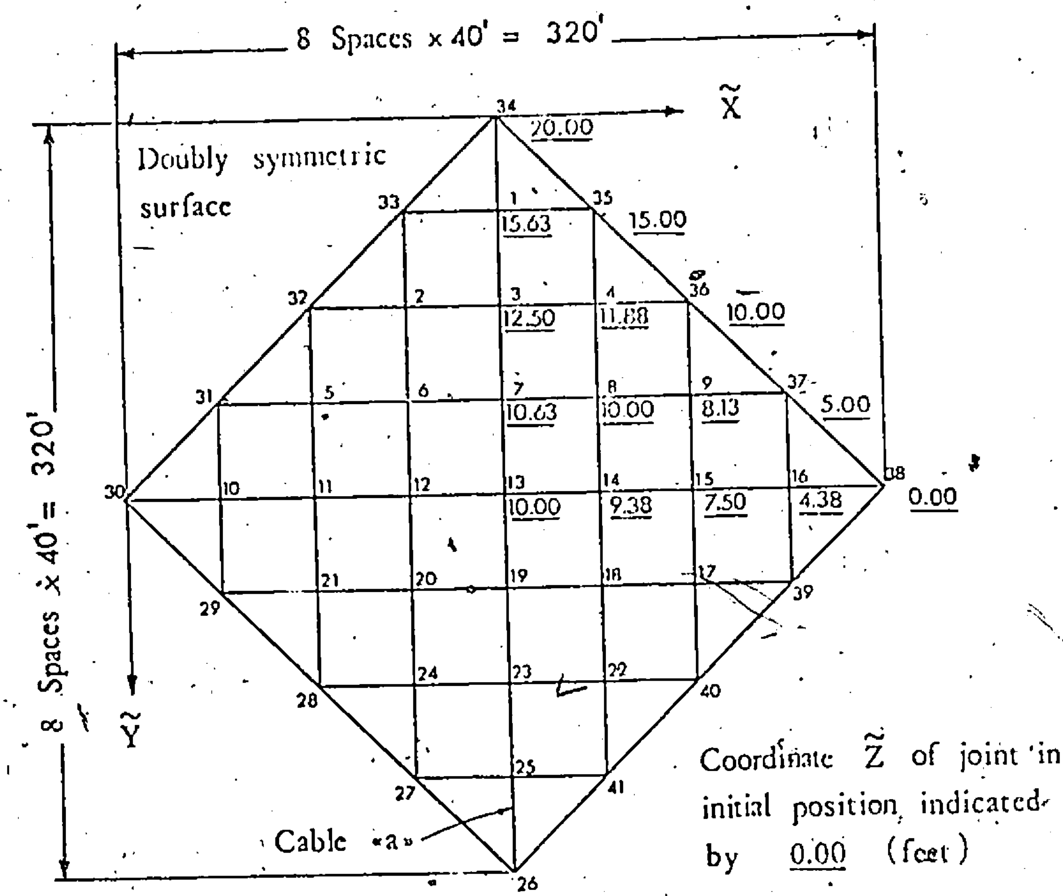

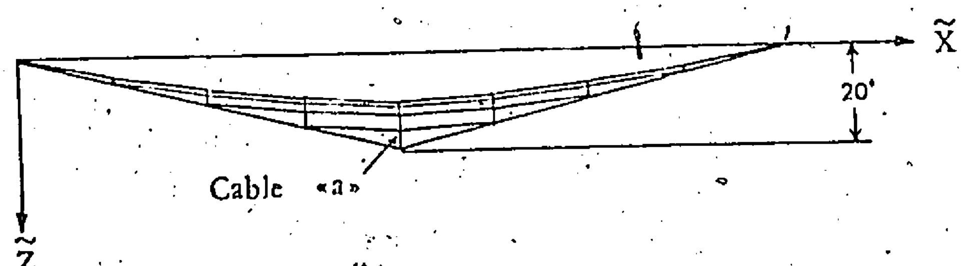

Figure 4. Example L1: Orthogonal Hyperbolic Paraboloid Net.

Reproduced with permission of the copyright owner. Further reproduction prohibited without permission.

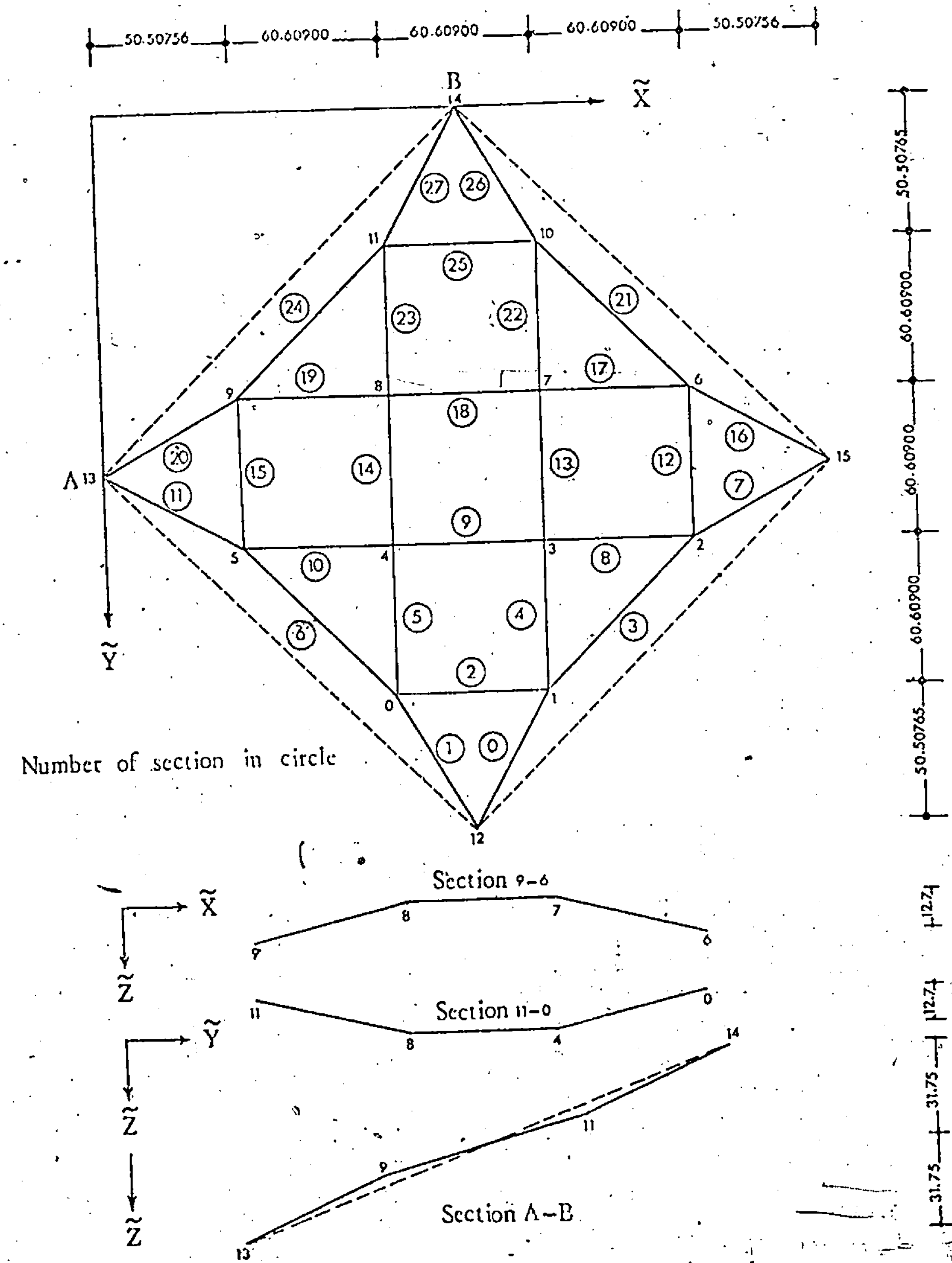

Figure 5. Example L2: Suspended Roof Structure Bounded by Main Cables.

Reproduced with permission of the copyright owner. Further reproduction prohibited without permission.

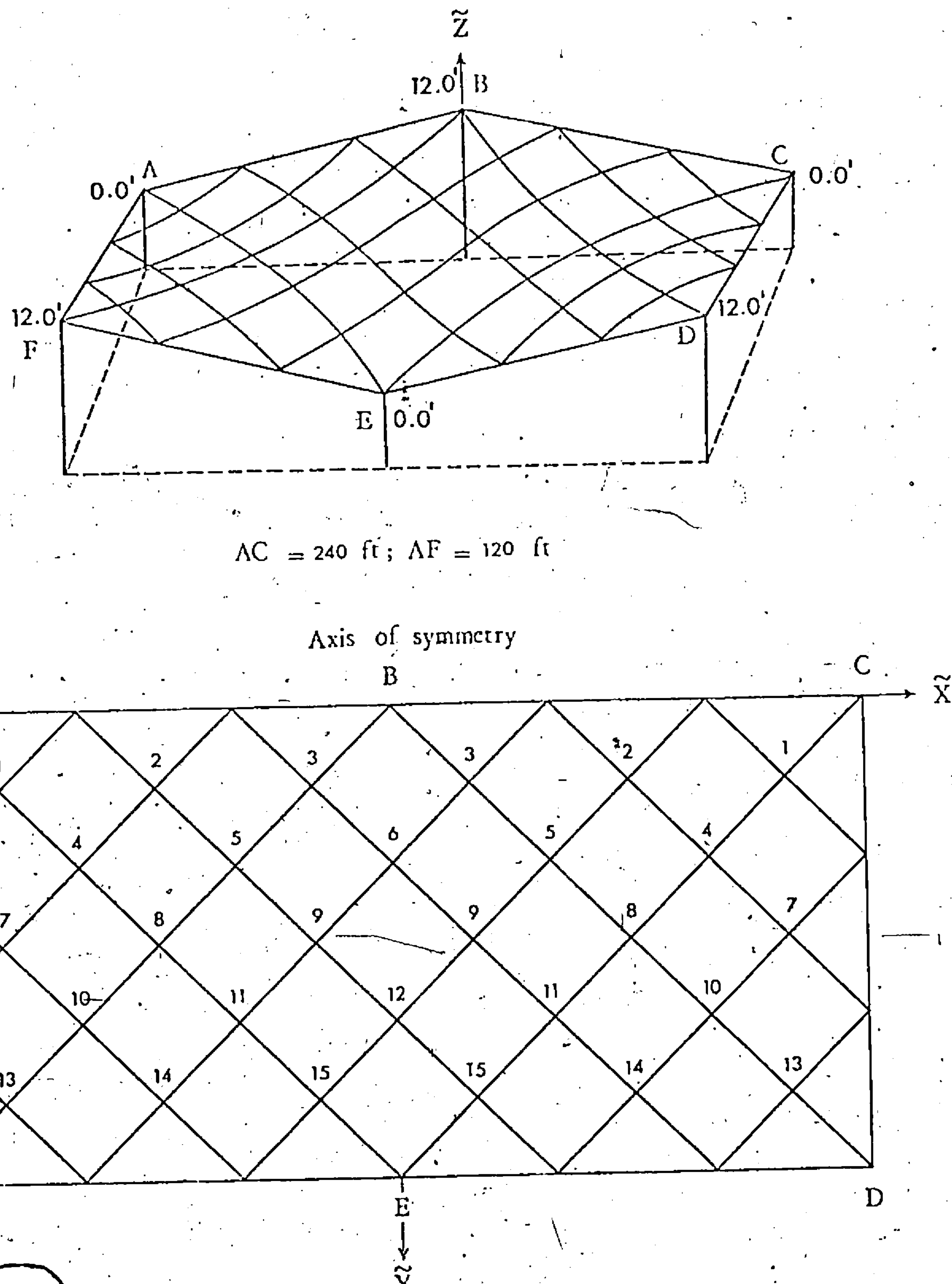

Figure 6. Example L3: Orthogonal Hyperbolic Paraboloid Cable-Net.

Reproduced with permission of the copyright owner. Further reproduction prohibited without permission.

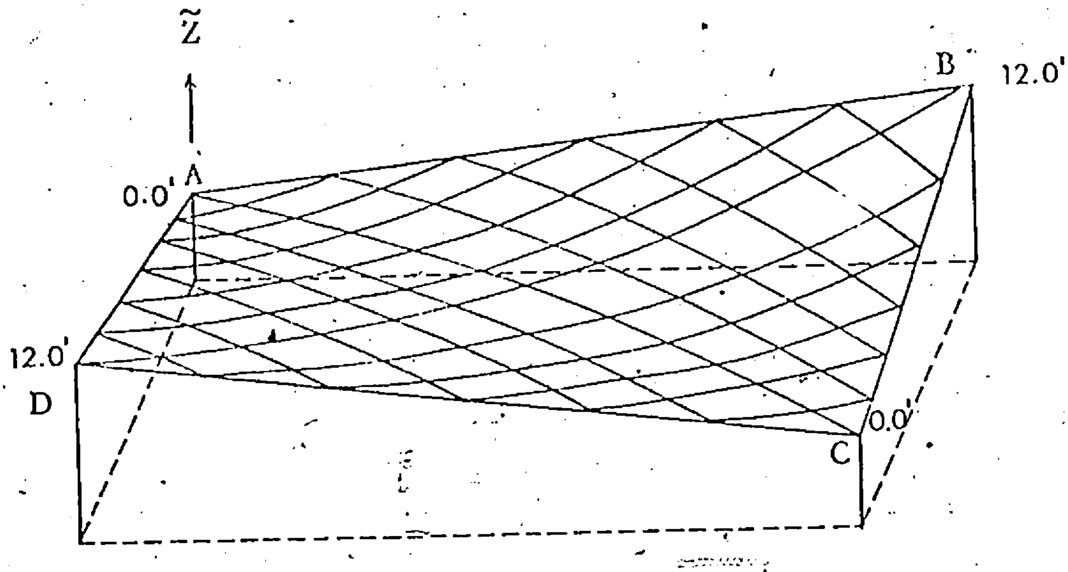

AB = 240 ft ; AD = 120 ft

AC is axis of antisymmetry

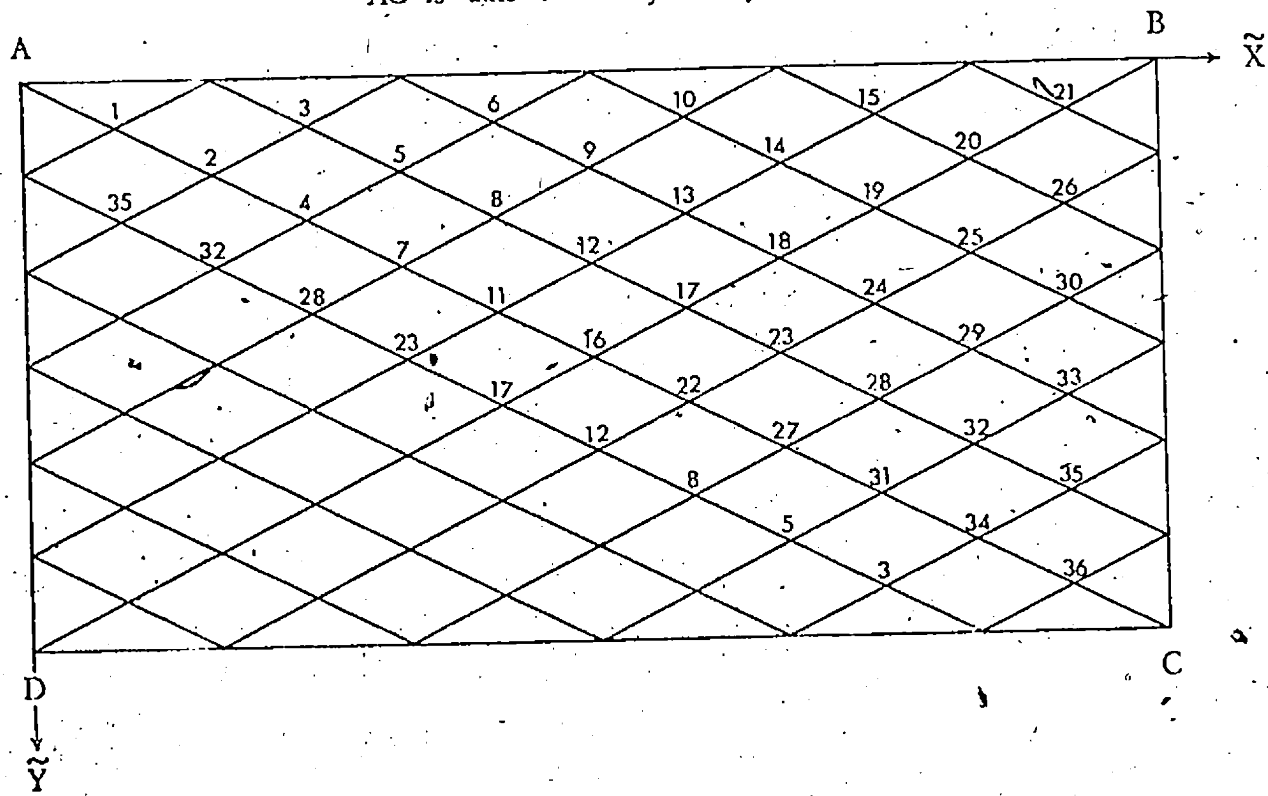

Figure 7. Example L4: Non-orthogonal Hyperbolic Paraboloid Cable Net.

Reproduced with permission of the copyright owner. Further reproduction prohibited without permission.

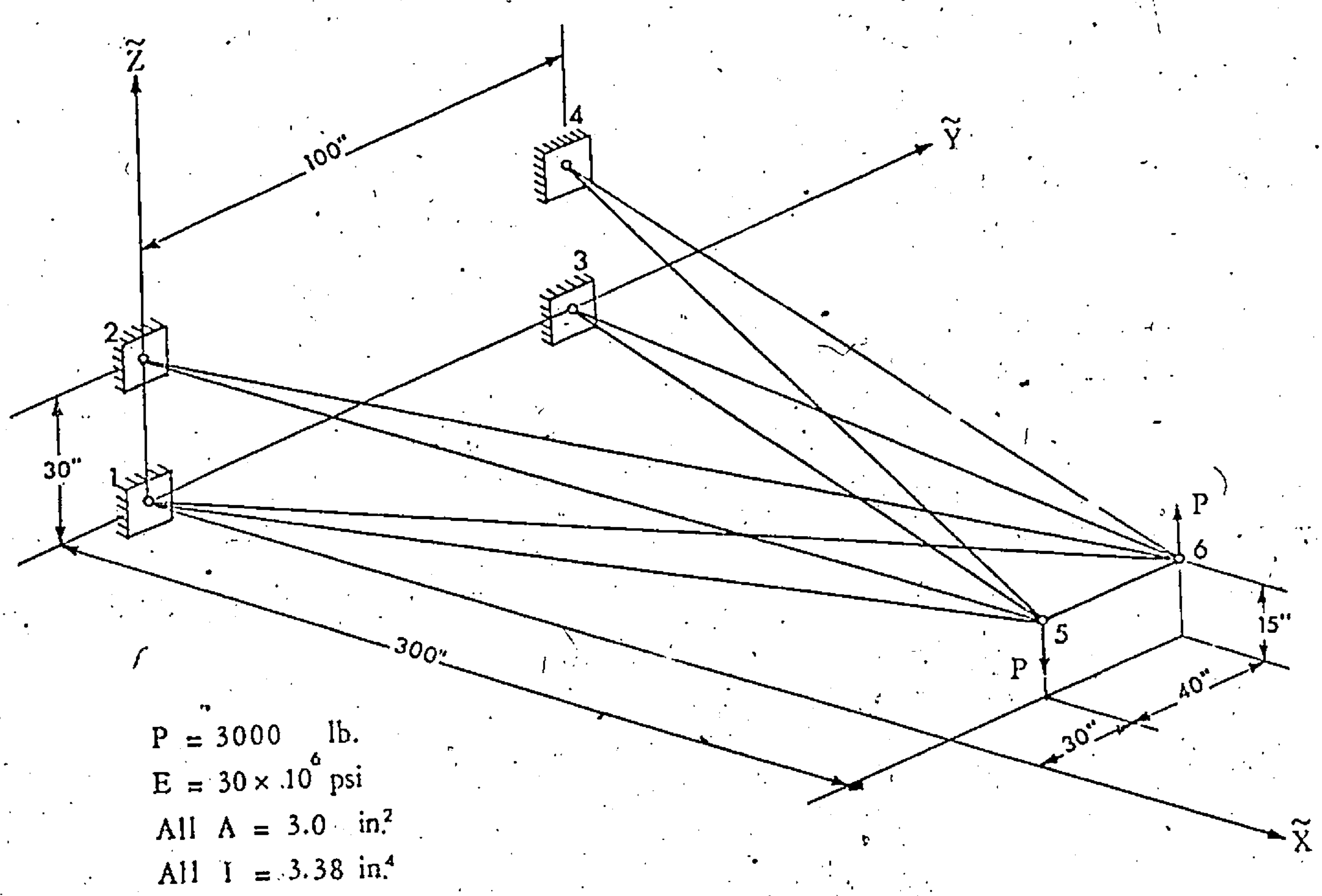

Figure 8. Cantilever Truss.

Reproduced with permission of the copyright owner. Further reproduction prohibited without permission.

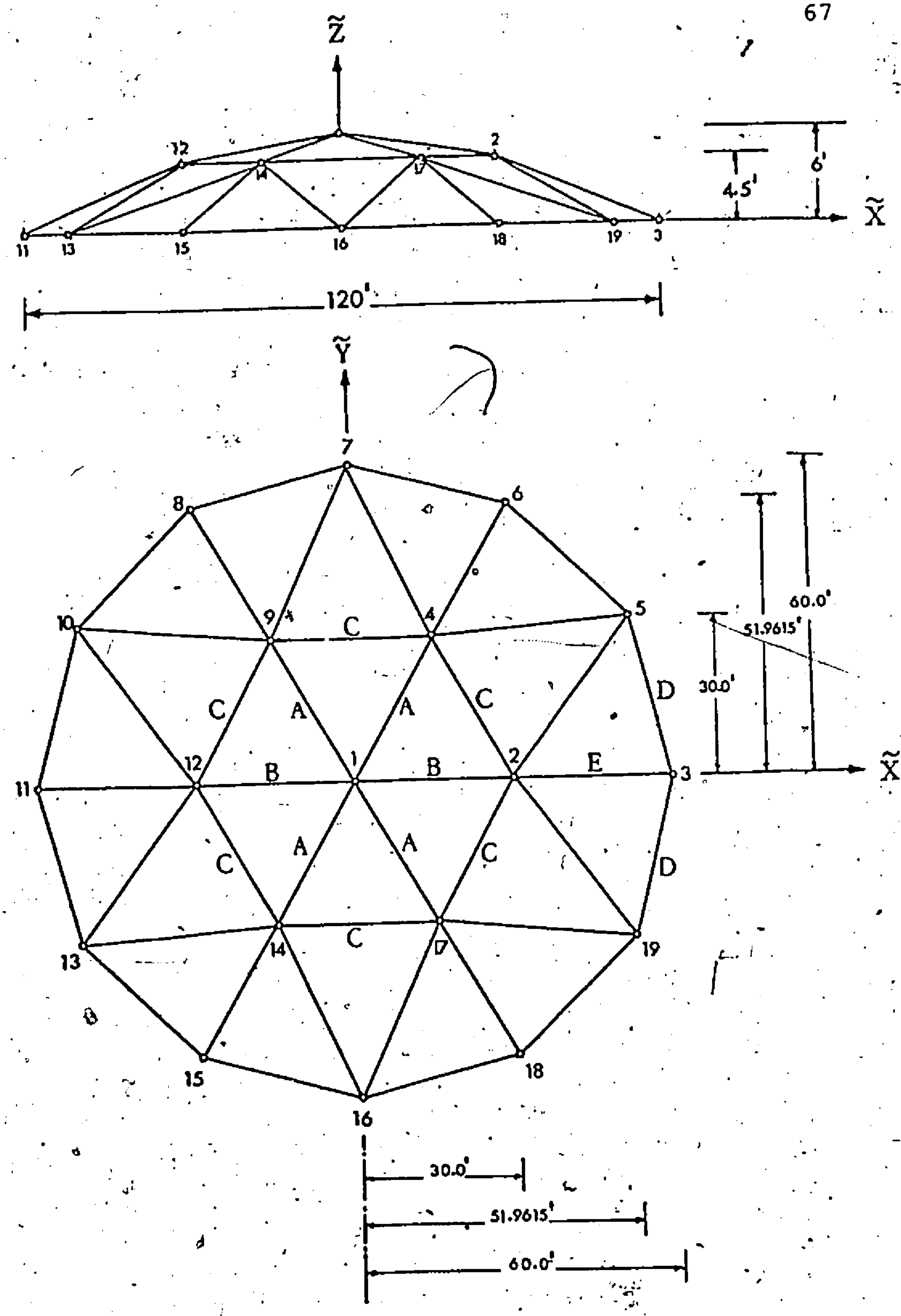

Figure 9. Suspended Shallow Truss Dome.

Reproduced with permission of the copyright owner. Further reproduction prohibited without permission.

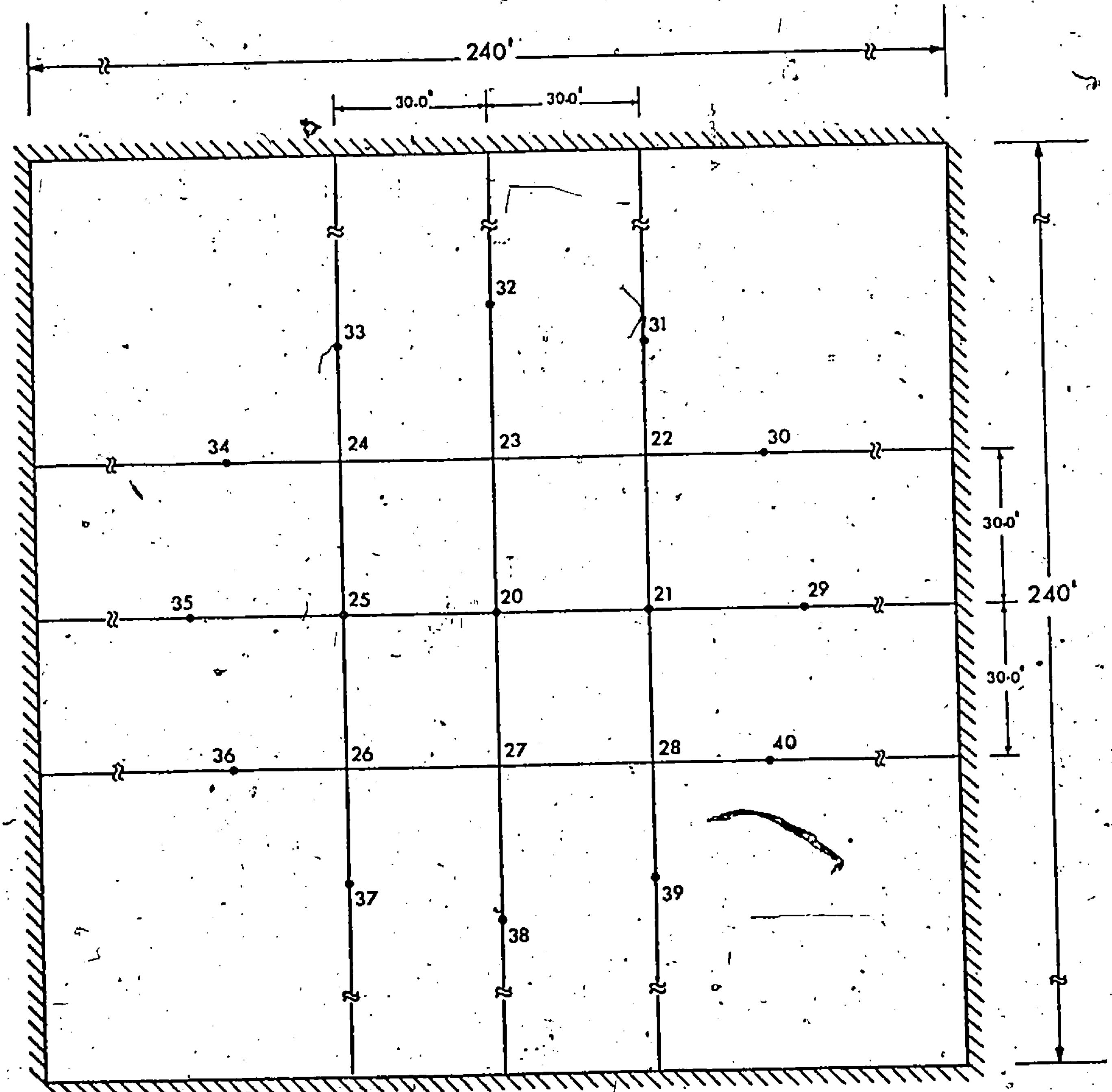

• Nodes of Carrying Hangers to Truss Dome

Figure 10. Horizontal Prestress Cable Network.

Reproduced with permission of the copyright owner. Further reproduction prohibited without permission.

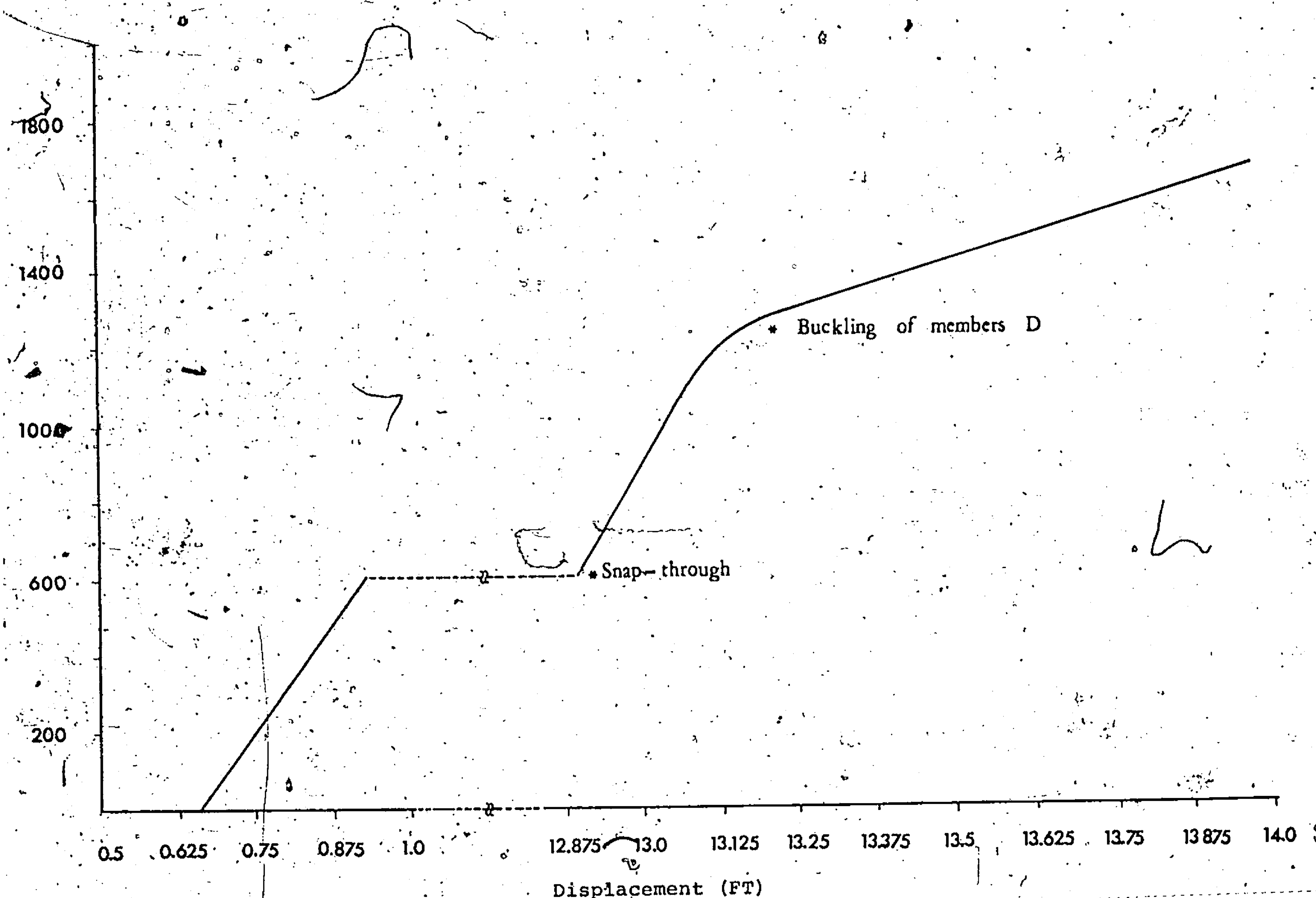

Figure 11. Load-Displacement History of Node 1. Case (i).

Reproduced with permission of the copyright owner. Further reproduction prohibited without permission.

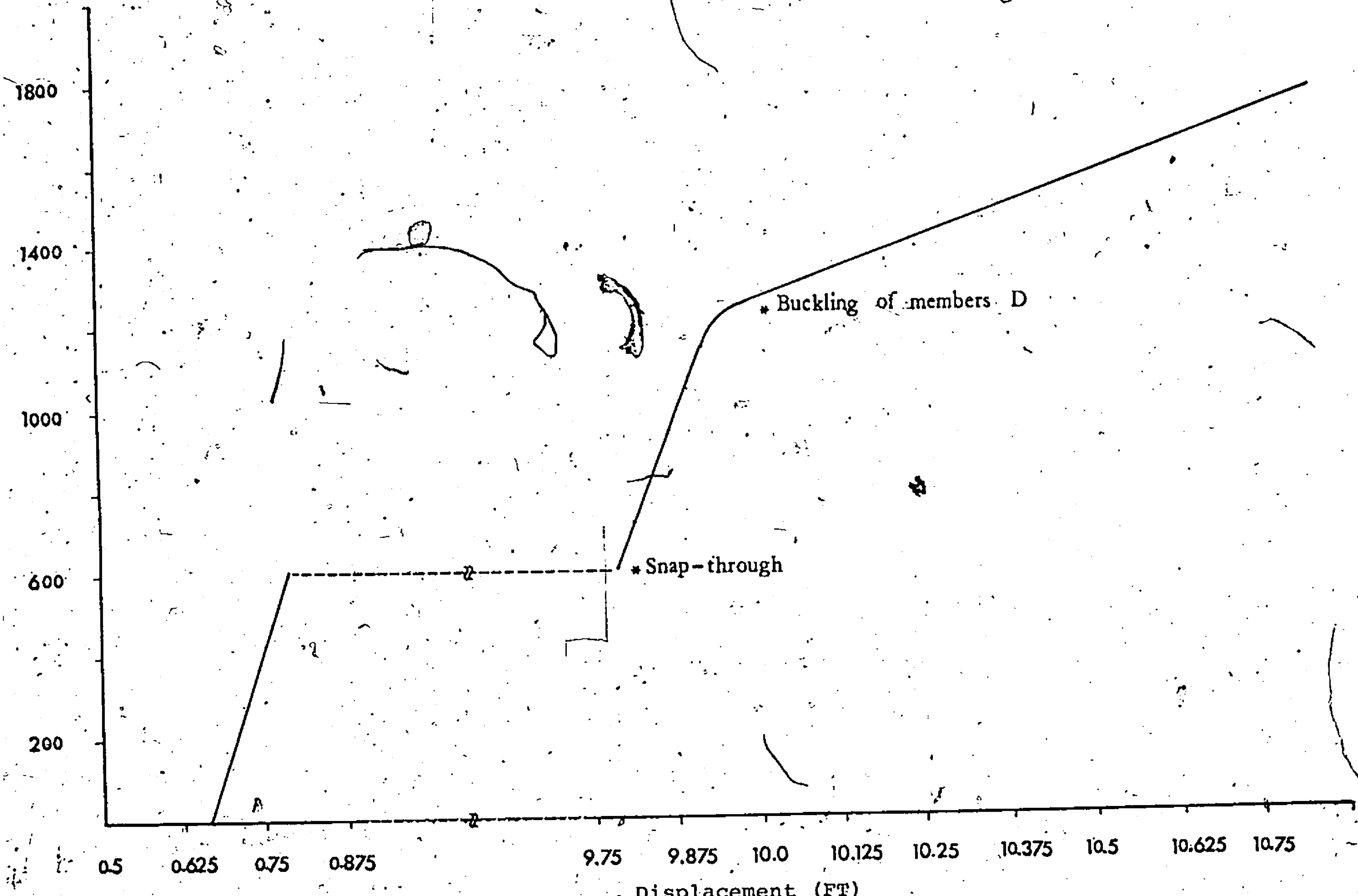

Figure 12. Load-Displacement History of Node 2. Case (i).

Reproduced with permission of the copyright owner. Further reproduction prohibited without permission.

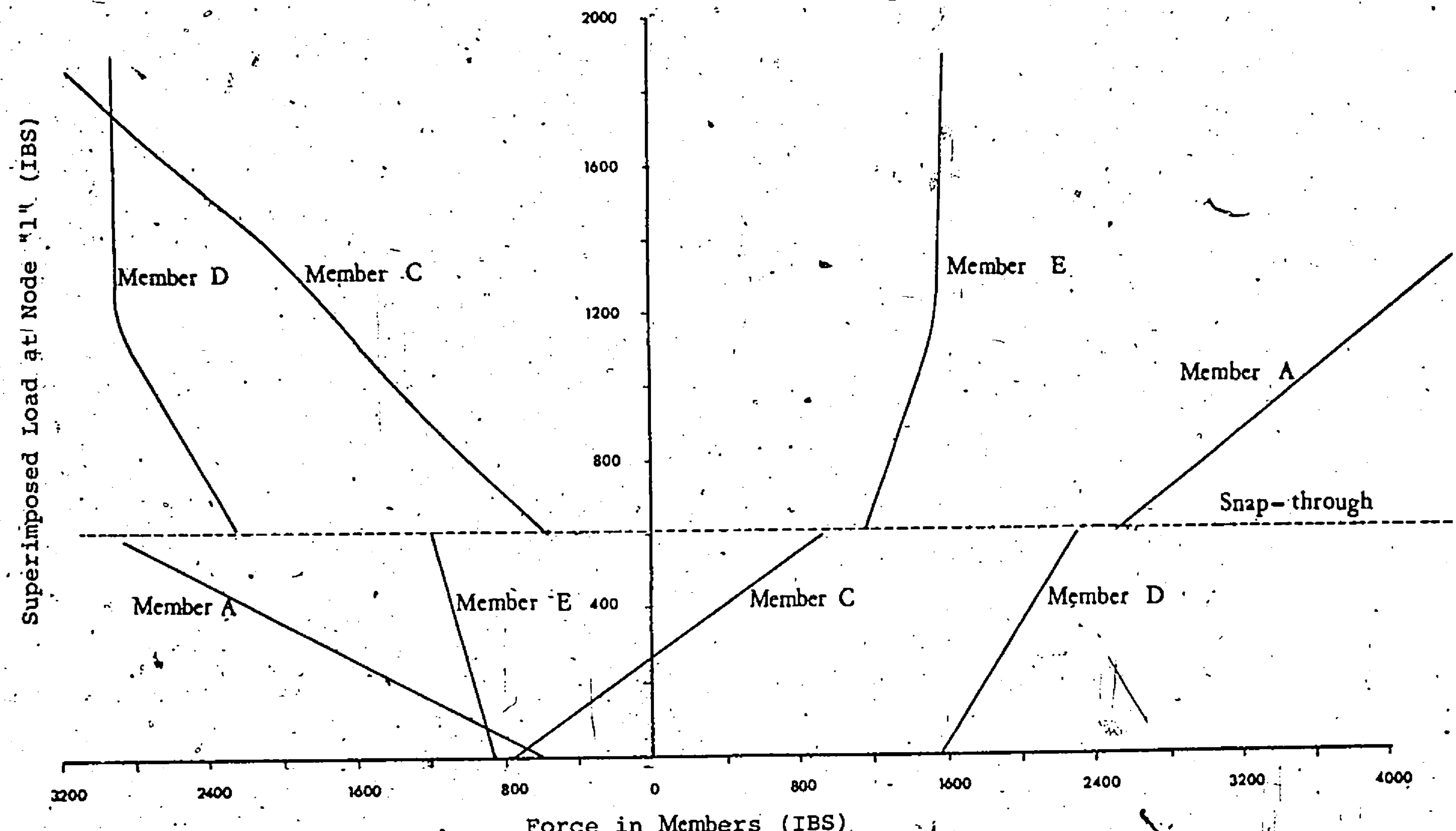

Figure 13. Load-force History of Members A, C, D and E. Case (i)

Reproduced with permission of the copyright owner. Further reproduction prohibited without permission.

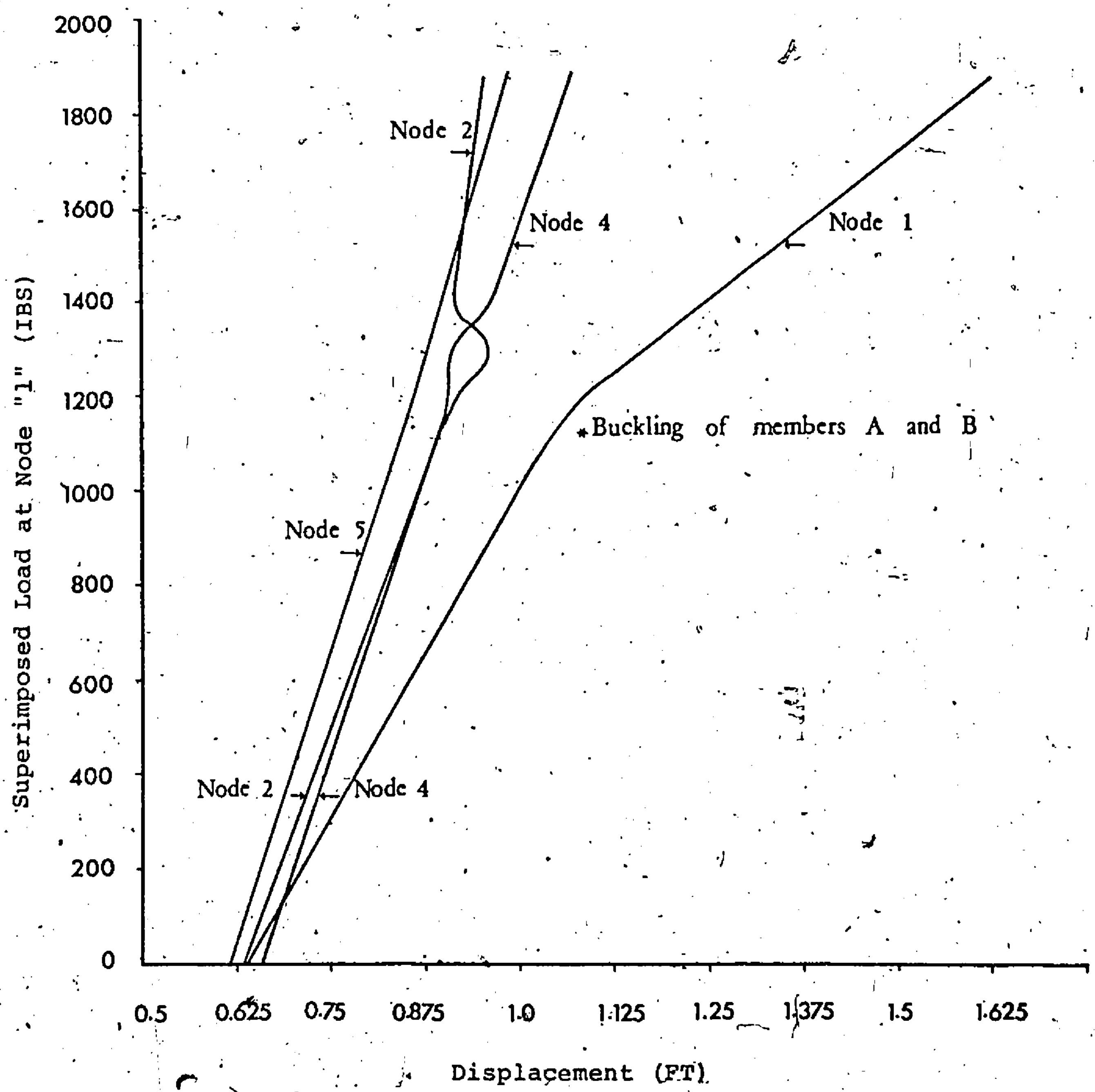

Figure 14. Load-Displacement History of Nodes 1, 2, 4 and 5, Case (ii).

Reproduced with permission of the copyright owner. Further reproduction prohibited without permission.

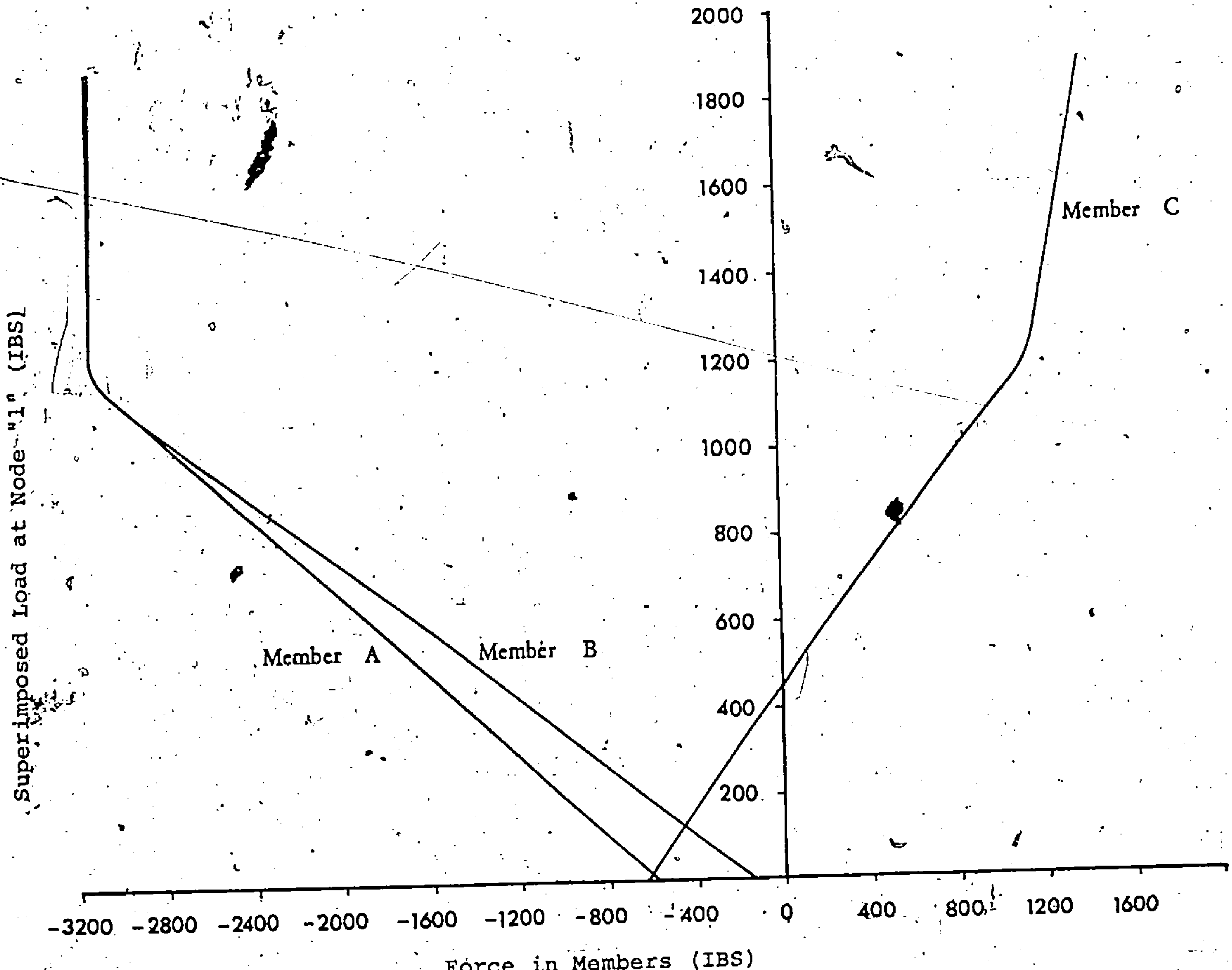

Figure 15. Load-Force History of Members A, B and C. Case (ii).

Reproduced with permission of the copyright owner. Further reproduction prohibited without permission.

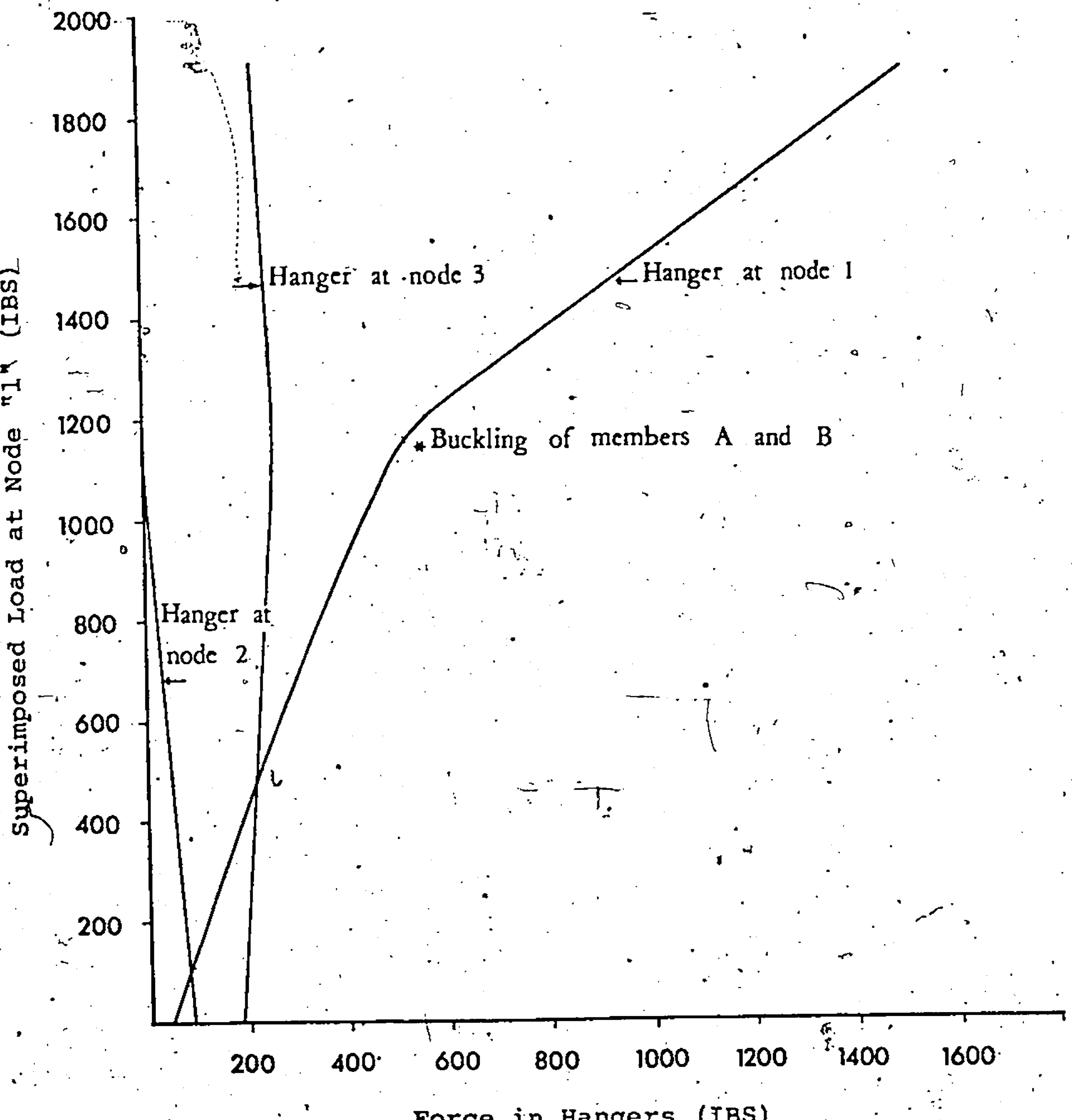

Figure 16. Forces in Hangers at Nodes 1, 2 and 3.
Case (ii).

Reproduced with permission of the copyright owner. Further reproduction prohibited without permission.

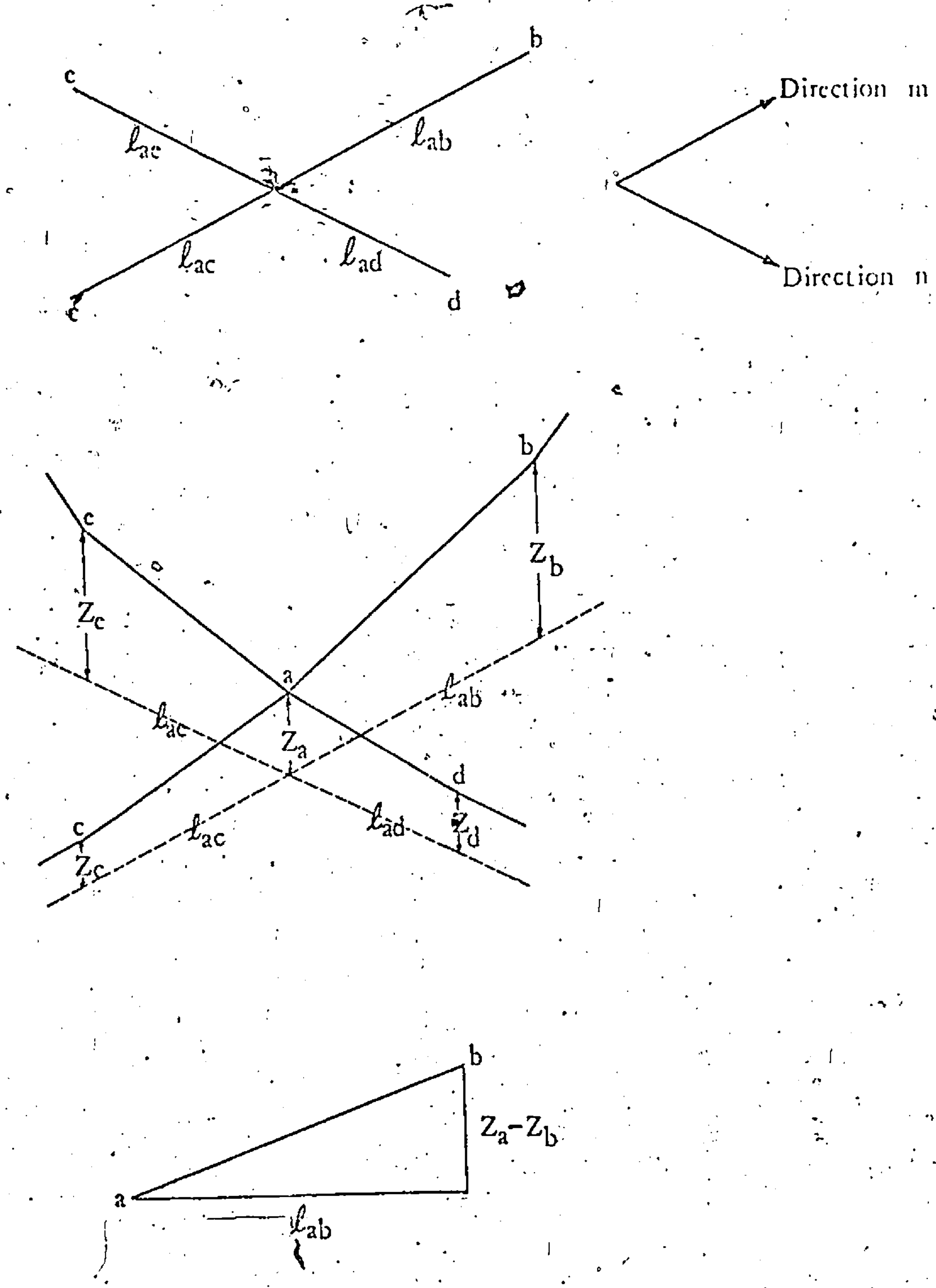

Figure B-1. General Joint "a" of a General Non-orthogonal Cable Net.

Reproduced with permission of the copyright owner. Further reproduction prohibited without permission.

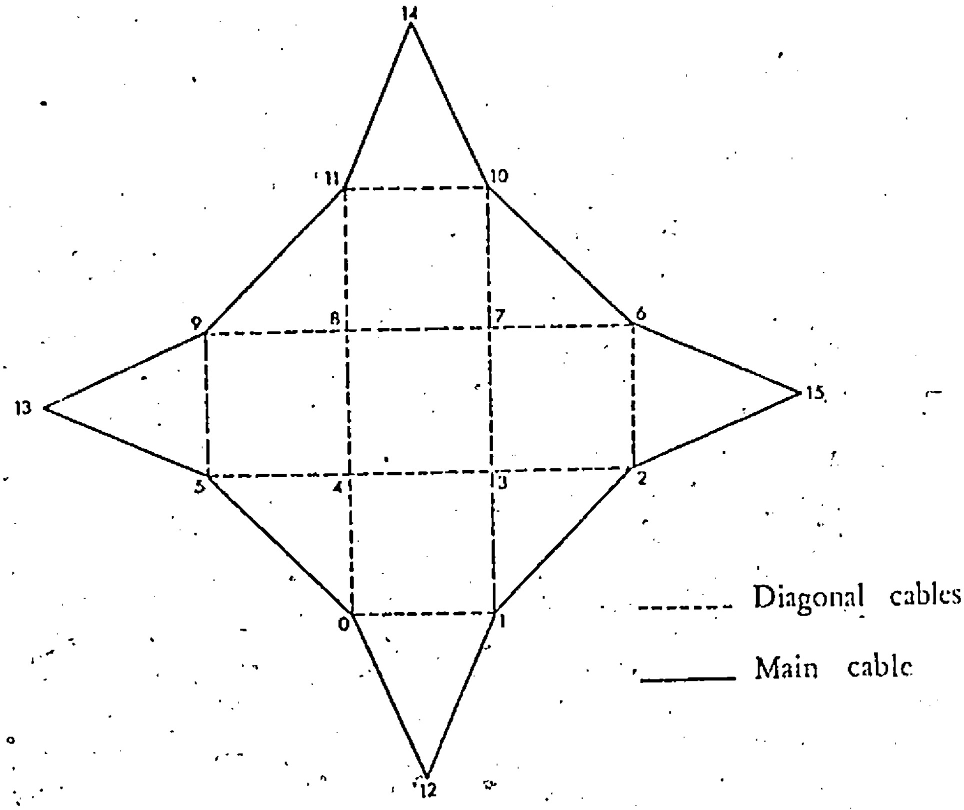

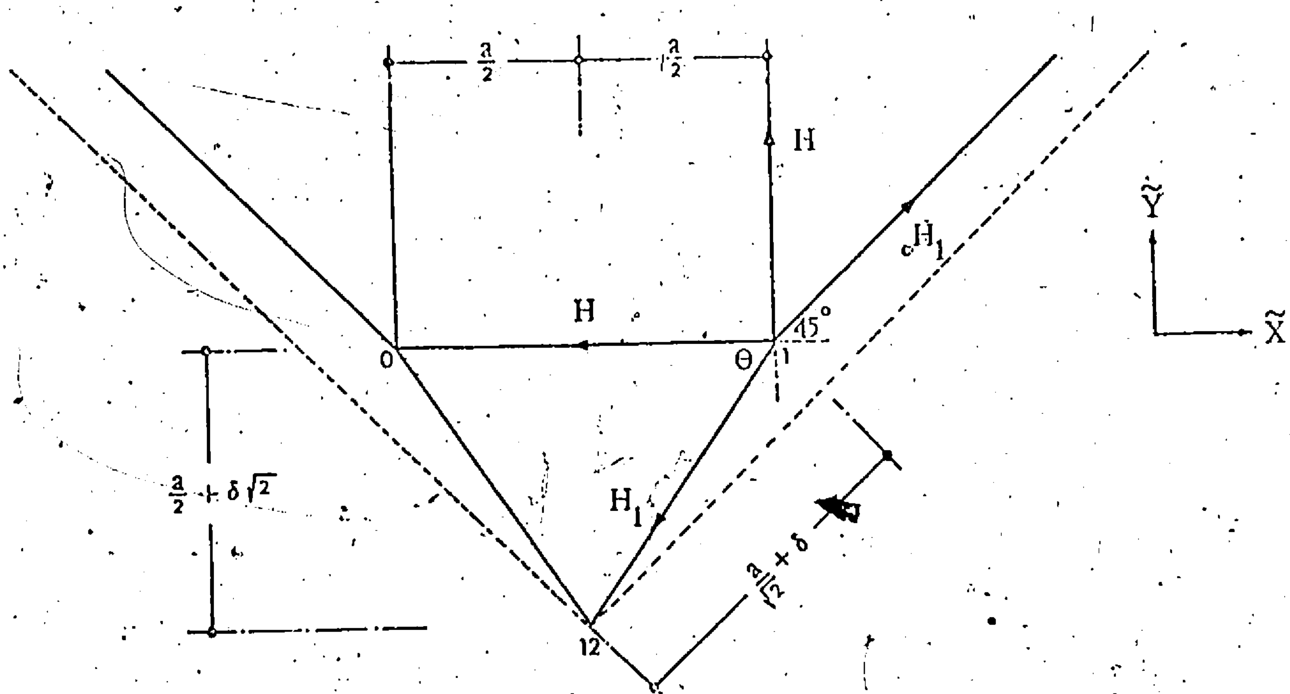

Figure C-1. General Joint of Suspended Roof in Example L2.

Reproduced with permission of the copyright owner. Further reproduction prohibited without permission.

TABLE 1

EXAMPLE L1 - Vertical Displacements of Cable "a" of Net Shown in Fig. 4 Under Vertical Loading

Joint Number	Vertical Displacement (feet)			
	Case (i)*		Case (ii)**	
	Thornton (Ref. 3)	Writer	Thornton (Ref. 3)	Writer
34	0.0	0.0	0.0	0.0
1	0.254	0.250	0.381	0.377
3	0.552	0.554	1.268	1.272
7	0.772	0.770	3.718	3.720
13	0.861	0.864	1.722	1.728
19	0.772	0.770	1.020	1.019
23	0.552	0.554	0.605	0.607
25	0.254	0.250	0.259	0.255
26	0.0	0.0	0.0	0.0

*Case (i): Vertical Load of 1 kip at Each Joint.

**Case (ii): Vertical Load of 1 kip at Each Joint Plus Additional Load of 14 kips at Joint 7.

Reproduced with permission of the copyright owner. Further reproduction prohibited without permission.

TABLE 2

EXAMPLE L1 - Results for Cable "a" of Net Shown in Fig. 4, Under Vertical and Horizontal Loading (Case iii)

Joint Number	Vertical Displacement (feet)		Member	Horizontal Components of Cable Tension (kips)	
	Thornton (Ref. 3)	Writer		Thornton (Ref. 3)	Writer
34	0.0	0.0	34-1	45.947	45.916
1	0.445	0.441	1-3	46.056	46.005
3	1.368	1.371	3-7	46.264	46.240
7	3.750	3.752	7-13	36.657	36.609
13	1.664	1.669	13-19	36.679	36.622
19	0.963	0.962	19-23	36.697	36.629
23	0.558	0.561	23-25	36.710	36.710
25	0.228	0.224	25-26	37.706	36.708
26	0.0	0.0	--	--	--

Reproduced with permission of the copyright owner. Further reproduction prohibited without permission.

TABLE 3

EXAMPLE L2 - Vertical Displacements of Joint "o" of Net Shown in Fig. 5 Under Vertical Load at the Same Joint (Case (i))

Load kg	Vertical Displacement (cms)		
	Siev (Ref. 2)		Writer
	Experiment	Theory	
0.2	0.200	0.213	0.214
0.4	0.393	0.432	0.426
0.6	0.592	0.630	0.632
0.8	0.784	0.833	0.836
1.0	0.973	1.032	1.035
1.2	1.163	1.224	1.227
1.4	1.348	1.411	1.415
1.6	1.530	1.593	1.597
1.8	1.713	1.768	1.772
2.0	1.895	1.937	1.941

Reproduced with permission of the copyright owner. Further reproduction prohibited without permission.

TABLE 4

EXAMPLE L2 - Displacements of Joints, Under Horizontal Loads of 0.2 kg (Case (ii)), And 1.0 kg (Case (iii)) at all Joints

	Joint Number	Displacements (cms)					
		in the $\tilde{X}$-direction		in the $\tilde{Y}$-direction		in the $\tilde{Z}$-direction	
		Siev (Ref. 2)	Writer	Siev (Ref. 2)	Writer	Siev (Ref. 2)	Writer
Case (ii)	0	0.0404	0.0408	-0.0079	-0.0092	0.0553	0.0565
	1	0.0402	0.0398	0.0063	0.0051	-0.0594	-0.0583
	2	0.0549	0.0538	-0.0003	-0.0007	-0.1293	-0.1307
	3	0.0528	0.0524	-0.0009	-0.0014	-0.1035	-0.1036
	4	0.0530	0.0536	0.0010	0.0006	0.1084	0.1085
	5	0.0526	0.0539	0.0002	0.0002	0.1237	0.1238
Case (iii)	0	0.2037	0.2044	-0.0513	-0.05[illegible]	0.2503	0.2516
	1	0.2007	0.2006	0.0153	0.0140	-0.3375	-0.3370
	2	0.3035	0.3031	-0.0019	-0.0023	-0.7174	-0.7205
	3	0.2631	0.2631	-0.0033	-0.0038	-0.4608	-0.4612
	4	0.2679	0.2688	0.0061	0.0056	0.5823	0.5833
	5	0.2428	0.2445	0.0004	0.0004	0.5664	0.5664

Reproduced with permission of the copyright owner. Further reproduction prohibited without permission.

TABLE 5

EXAMPLE L2 - Tension in Sections (kgs) for Loading Cases (ii) and (iii)

Section Number	Case (ii)		Case (iii)	
	Siev (Ref. 2)	Writer	Siev (Ref. 2)	Writer
0	24.502	24.423	21.254	21.174
1	26.358	26.281	30.383	30.308
2	4.145	4.139	4.140	4.133
3	23.529	23.462	20.039	19.968
4	4.123	4.106	3.822	3.806
5	4.369	4.353	5.013	4.998
6	25.423	25.355	29.401	29.334
7	24.190	24.113	19.755	19.676
8	4.046	4.029	3.485	3.469
9	4.159	4.143	4.411	4.396
10	4.453	4.437	5.522	5.506
11	26.681	26.604	32.118	32.043
12	4.112	4.105	3.920	3.912
13	4.036	4.020	3.743	3.727
14	4.275	4.260	4.900	4.885
15	4.172	4.166	4.194	4.187

Reproduced with permission of the copyright owner. Further reproduction prohibited without permission.

TABLE 6

EXAMPLE L3 - Vertical Displacements of the Cable Roof Shown in Fig. 6 Under Vertical Loading (1 kip/joint)

Joint Number	Vertical Displacement (ft.)	
	Kumanan (Ref. 4)	Writer
1	-0.097225	-0.097918
2	-0.218935	-0.216730
3	-0.326019	-0.318829
4	-0.208622	-0.208971
5	-0.411922	-0.407352
6	-0.618200	-0.604488
7	-0.149592	-0.149587
8	-0.307045	-0.306545
9	-0.645787	-0.683722
10	-0.212964	-0.213448
11	-0.432823	-0.427226
12	-0.656570	-0.639941
13	-0.101908	-0.102647
14	-0.226937	-0.224849
15	-0.358106	-0.347196

Reproduced with permission of the copyright owner. Further reproduction prohibited without permission.

TABLE 7

EXAMPLE L4 – Vertical Displacements of the Non-orthogonal Cable Roof Shown in Fig. 7 Under Vertical Loading (1 kip/joint)

Joint No.	Vertical Displacements (ft)	
	Kumanan (Ref. 5)	Writer
1	-0.205983	-0.196013
2	-0.518198	-0.500102
3	-0.382553	-0.370509
4	-0.829292	-0.807666
5	-0.732224	-0.714396
6	-0.450873	-0.441454
7	-1.088215	-1.068485
8	-1.014998	-0.997858
9	-0.801635	-0.790219
10	-0.458200	-0.453151
11	-1.262860	-1.248153
12	-1.203370	-1.190767
13	-1.031159	-1.023062
14	-0.756990	-0.753920
15	-0.401313	-0.401787
16	-1.328606	-1.317547
17	-1.273480	-1.264430
18	-1.115296	-1.110431
19	-0.866189	-0.866219
20	-0.551684	-0.555793
21	-0.224608	-0.230291
22	-1.262858	-1.248153
23	-1.202629	-1.190082
24	-1.029952	-1.021963
25	-0.755783	-0.752861
26	-0.400632	-0.401203
27	-1.088214	-1.068485
28	-1.013703	-0.996631
29	-0.799682	-0.788393
30	-0.456666	-0.451754
31	-0.829292	-0.807665
32	-0.730763	-0.712964
33	-0.449147	-0.439788
34	-0.518198	-0.500102
35	-0.381486	-0.369412
36	-0.205985	-0.196013

Reproduced with permission of the copyright owner. Further reproduction prohibited without permission.

TABLE 8

Force Distribution (lbs) of the Truss Shown in Fig. 8

Truss Member	None	Nonlinearity Included			
		Finite Node Displ.		Finite Node Displ. + Local Buckling	
		Ref. 6	Writer	Ref. 6	Writer
1-5*	-15,580	-14,070	-14,073	-11,030	-11,002
1-6	+14,920	+13,410	+13,408	-4,430	-4,544
2-5	+15,580	+16,620	+16,630	+25,740	+25,843
2-6*	-14,920	-16,010	-16,006	-10,590	-10,545
3-5*	-14,920	-16,000	-16,006	-10,600	-10,545
3-6	+15,580	+16,630	+16,630	+25,740	+25,843
4-5	+14,920	+13,410	+13,408	-4,410	-4,544
4-6*	-15,580	-14,070	-14,073	-11,040	-11,002
5-6	0	+850	+846	+4,920	+4,981

*Buckled truss member.

Reproduced with permission of the copyright owner. Further reproduction prohibited without permission.

TABLE 9

Node Displacements (Inches) of the Truss Shown in Fig. 8

Displacement	Nonlinearity Included				
	None	Finite Node Disp.		Finite Node Disp. + Local Buckling	
		Ref. 6	Writer	Ref. 6	Writer
$\tilde{u}^{(5)}$	0.0	0.0	0.0	-0.134	-0.140
$\tilde{v}^{(5)}$	0.0	+0.027	+0.027	+0.307	+0.309
$\tilde{w}^{(5)}$	-1.052	-1.036	-1.036	-3.414	-3.513
$\tilde{u}^{(6)}$	0.0	0.0	0.0	-0.144	-0.140
$\tilde{v}^{(6)}$	0.0	-0.027	-0.027	-0.307	-0.309
$\tilde{w}^{(6)}$	+1.052	+1.036	+1.036	+3.586	+3.513

Reproduced with permission of the copyright owner. Further reproduction prohibited without permission.

REFERENCES

1. Siev, A., "A General Analysis of Prestressed Nets", International Association for Bridge and Structural Engineering, Vol. 23, 1963, pp. 283-293.

2. Siev, A., "Prestressed Suspended Roofs Bounded by Main Cables", International Association for Bridge and Structural Engineering, Vol. 27, 1967, pp. 171-185.

3. Thornton, C.H. and Birnstiel, C., "Three-Dimensional Suspension Structures", Journal of the Structural Division, ASCE, ST2, April 1967, pp. 247-270.

4. Kumanan, T., "Elastic and Inelastic Analysis of Pretensioned Cable-Roof Structures", Ph.D. Thesis, The Faculty of Graduate Studies, University of Windsor, (1971).

5. Kumanan, T., "Analysis of Nonorthogonal Cable Roofs", M.A.Sc. Thesis, The Faculty of Graduate Studies, University of Windsor, (1969).

6. Bogner, F.K., Mallet, R.H., Minich, M.D., and Schmit, L.A., "Development and Evaluation of Energy Search Methods of Nonlinear Structural Analysis", AFFDL-TR-65-113, Air Force Flight Dynamics Laboratory, Wright-Patterson Air Force Base, Ohio (1965).

7. Mallet, R.H. and Berke, L., "Automated Methods for the Finite Displacement Analysis of Three-Dimensional Truss and Frame Assemblies", AFFDL-TR-66-102, Air Force Flight Dynamics Laboratory, Wright-Patterson Air Force Base, Ohio (1966).

8. Bogner, F.K., "Analysis of Tension Structures", AFFDL-TR-68-150, Air Force Flight Dynamics Laboratory, Wright-Patterson Air Force Base, Ohio (1968).

Reproduced with permission of the copyright owner. Further reproduction prohibited without permission.

9. Fletcher, R. and Powell, M.J.D., "A Rapidly Convergent Descent Method for Minimization", Computer Journal, Vol. 6, 1963, pp. 163-168.

10. Buchholdt, H.A., "Deformation of Prestressed Cable Nets", Acta Polytechnica Scandinavica, Civil Engineering and Building Construction Series, No. 38, Torondheim (1966).

11. Buchholdt, H.A., Das, N.K. and Al-Hilli, A.J., "A Gradient Method for the Analysis of Cable Structures with Flexible Boundaries", International Conference on Tension Roof Structures, London, April 1974.

12. Greenberg, D.P., "Inelastic Analysis of Suspension Roof Structures", Journal of the Structural Division, ASCE, ST5, May 1970, pp. 905-931.

13. Jonatowski, J.J. and Birnstiel, C., "Inelastic Stiffened Suspension Space Structures", Journal of the Structural Division, ASCE, ST6, June 1970, pp. 1143-1166.

14. Schmit, L.A., Bogner, F.K. and Fox, R.L., "Finite Deflection Structural Analysis Using Plate and Shell Discrete Elements", AIAA Journal, Vol. 6, No. 5, May 1968, pp. 781-791.

15. Fletcher, R. and Reeves, C.M., "Function Minimization by Conjugate Gradients", Computer Journal, Vol. 7, 1964, pp. 149-154.

16. Fox, R.L., <u>Optimization Methods for Engineering Design</u>, Addison-Wesley Publishing Company, 1971.

17. Fox, R.L. and Stanton, E., "Developments in Structural Analysis by Direct Energy Minimization", AIAA Journal, Vol. 6, No. 6, June 1968, pp. 1036-1042.

Reproduced with permission of the copyright owner. Further reproduction prohibited without permission.

APPENDIX A

GENERAL TRUSS FINITE ELEMENT FORMULATIONS

I. Linear Elastic Analysis of Tension Members

A typical truss tension member in the undeformed and deformed states is shown in Fig. 1. The initial undeformed length is given by

$$L = [(\tilde{X}_q - \tilde{X}_p)^2 + (\tilde{Y}_q - \tilde{Y}_p)^2 + (\tilde{Z}_q - \tilde{Z}_p)^2]^{\frac{1}{2}} \qquad \text{(A-1)}$$

The deformed length is given by

$$S = \{[(\tilde{X}_q + \tilde{u}_q) - (\tilde{X}_p + \tilde{u}_p)]^2 + [(\tilde{Y}_q + \tilde{v}_q) - (\tilde{Y}_p + \tilde{v}_p)]^2$$

$$+ [(\tilde{Z}_q + \tilde{w}_q) - (\tilde{Z}_p + \tilde{w}_p)]^2\}^{\frac{1}{2}} \qquad \text{(A-2)}$$

The location of the member joints p and q in the initial position are given by $\tilde{X}_p$, $\tilde{Y}_p$, $\tilde{Z}_p$, $\tilde{X}_q$, $\tilde{Y}_q$ and $\tilde{Z}_q$ coordinates, measured with respect to the reference coordinate system $(\tilde{X},\tilde{Y},\tilde{Z})$. Note that $\tilde{u}$, $\tilde{v}$, and $\tilde{w}$ are the displacement components of the member joints in the $\tilde{X}$, $\tilde{Y}$, and $\tilde{Z}$ directions respectively.

The strain-deformation relation is expressed in terms of the axial deformation (u), measured along the deformed length of the member (x-direction), and is given

Reproduced with permission of the copyright owner. Further reproduction prohibited without permission.

by

$$\varepsilon = u_x \tag{A-3}$$

Integration of the strain energy definition

$$dU = \int_0^{\varepsilon+\varepsilon_p} \sigma \, d\varepsilon \tag{A-4}$$

under the assumption of ideal linear elastic material behaviour

$$\sigma = E(\varepsilon + \varepsilon_p) \tag{A-5}$$

results in the following expression for the strain energy in terms of the strain

$$U = \frac{E}{2} \int_V (\varepsilon + \varepsilon_p)^2 \, dV \tag{A-6}$$

Substitution for the strain from Eq. A-3 and integrating over the cross-section yields the strain energy in terms of u

$$U = \frac{AE}{2} \int_0^S (u_x + \varepsilon_p)^2 \, dx \tag{A-7}$$

From the fundamentals of the calculus of variations, the actual displacement state is the one for which the first variation of the strain energy is zero;

Reproduced with permission of the copyright owner. Further reproduction prohibited without permission.

$$\delta U = 0 = \frac{AE}{2} \int_0^S 2\, u_x\, \delta u_x\, dx + \frac{AE}{2} \int_0^S 2\delta u_x\, \varepsilon_p\, dx$$

Integrating by parts

$$\delta U = 0 = AE \left\{ \left| u_x\, \delta u \right|_0^S - \int_0^S \frac{du_x}{dx}\, \delta u\, dx \right\}$$

$$+ AE \left\{ \left| \varepsilon_p\, \delta u \right|_0^S - \int_0^S \frac{d\varepsilon_p}{dx}\, \delta u\, dx \right\}$$

or

$$\delta U = 0 = -EA \int_0^S \left\{ \frac{d}{dx}(u_x + \varepsilon_p) \right\} \delta u\, dx \quad \text{(a)}$$

$$+ EA \left| (u_x + \varepsilon_p)\, \delta u \right|_0^S \quad \text{(b)} \qquad \text{(A-8)}$$

Each of the contributions (a) and (b) in Eq. A-8 must be individually equal to zero, since the variation δu is arbitrary; this gives

$$\frac{d}{dx}(u_x + \varepsilon_p) = 0 \qquad \text{(A-9)}$$

which represents the governing differential equation for the problem. By integration,

$$u_x + \varepsilon_p = K_1 \qquad \text{(A-10)}$$

Reproduced with permission of the copyright owner. Further reproduction prohibited without permission.

From Fig. 1, it is apparent that the imposed boundary conditions are

$$u\Big|_{x=0} = 0 \quad \text{and} \quad u\Big|_{x=S} = S-L \qquad \text{(A-11)}$$

Also, the variational quantity δu must vanish at the ends of the member, therefore, Eq. A-8(b) and Eq. A-10 indicate that the force in the member is constant and given by

$$F = AEK_1 \qquad \text{(A-12)}$$

The constant K_1 can be determined by integrating Eq. A-10 over the length S:

$$\int_0^S K_1\, dx = \int_0^S (u_x + \varepsilon_p)\, dx$$

or

$$K_1 = 1 - \frac{L}{S} + \varepsilon_p \qquad \text{(A-13)}$$

Substituting Eq. A-10 into Eq. A-7 and performing the indicated integration, the tension element strain energy is given by

$$U = \frac{AE}{2} S\, K_1^2 \qquad \text{(A-14)}$$

Reproduced with permission of the copyright owner. Further reproduction prohibited without permission.

II. Inelastic Analysis of Tension Members

The stress-strain relationship between the proportional limit and the point of ultimate stress (Fig. 2) is given by

$$\sigma = \frac{-2f + \sqrt{4f^2 - 4(2g\varepsilon + c)}}{2} \qquad \text{(A-15)}$$

The strain-deformation relation is given by

$$\varepsilon = u_x + \tfrac{1}{2} u_x^2 \qquad \text{(A-16)}$$

Integrating the strain energy density definition gives

$$dU = \tfrac{1}{2}E\varepsilon_e^2 + \int_{\varepsilon_e}^{\varepsilon+\varepsilon_p} \sigma \, d\varepsilon \qquad \text{(A-17)}$$

After substituting the stress σ from Eq. A-15 the following expression of the element strain energy in terms of the strain is obtained

$$U = \int_V \Big\{ \tfrac{1}{2}E\varepsilon_e^2 + f\,\varepsilon_e + \frac{1}{24g}(-8g\,\varepsilon_e + 4f^2 - 4c)^{3/2}$$

$$- f(\varepsilon + \varepsilon_p) - \frac{1}{24g}\left[-8g(\varepsilon + \varepsilon_p) + 4f^2 - 4c\right]^{3/2} \Big\}\, dV$$

$$\text{(A-18)}$$

Reproduced with permission of the copyright owner. Further reproduction prohibited without permission.

where ε_e is the strain at the proportional limit.

Substituting for the strain from Eq. A-16 and integrating over the cross-section:

$$U = AS\left[\tfrac{1}{2}E\varepsilon_e^2 + f\,\varepsilon_e + \frac{1}{24g}\,(-8g\,\varepsilon_e + 4f^2 - 4c)^{3/2}\right]$$

$$- A\int_0^S f(u_x + \tfrac{1}{2}u_x^2 + \varepsilon_p)\,dx - A\int_0^S \frac{1}{24g}\,B^{3/2}\,dx \qquad \text{(A-19)}$$

where the term B is given as:

$$B = -8g(u_x + \tfrac{1}{2}u_x^2 + \varepsilon_p) + 4f^2 - 4c \qquad \text{(A-20)}$$

The following expression is obtained after taking the first variation of Eq. A-19, integration by parts and rearranging terms:

$$\delta U = 0 = A\int_0^S \left\{\frac{d}{dx}\left[\left(-\frac{f}{2} + \tfrac{1}{2}B^{1/2}\right)(1 + u_x)\right]\right\}\delta u\,dx \qquad \text{(a)}$$

$$+ A\left|\left\{\left(-\frac{f}{2} + \tfrac{1}{2}B^{1/2}\right)(1 + u_x)\right\}\delta u\right|_0^S \qquad \text{(b)}$$

where B is given by Eq. A-20.

Each of the contributions (a) and (b) in Eq. A-21 must be equal to zero, since the variation δu is arbitrary.

Reproduced with permission of the copyright owner. Further reproduction prohibited without permission.

Thus,

$$\frac{d}{dx}\left[\left(-\frac{f}{2} + \tfrac{1}{2} B^{\frac{1}{2}}\right)(1 + u_x)\right] = 0 \qquad \text{(A-22)}$$

which represents the governing differential equation for this case; by integration, the expression between brackets is equal to a constant, and as the quantities f, g, c and ε_p are constants, it follows that;

$$u_x = K_2 = \text{constant} \qquad \text{(A-23)}$$

Also, the variational quantity δu must vanish at the ends of the member. Equations A-21(b) and A-23 indicate that the force in the member is constant and given by

$$F = A\left[-\frac{f}{2} + \tfrac{1}{2}\left[-8g\left(K_2 + \tfrac{1}{2}K_2^2 + \varepsilon_p\right) + 4f^2 - 4c\right]^{\frac{1}{2}}\right](1 + K_2)$$

(A-24)

The constant K_2 can be determined by integrating Eq. A-23 over the length S and incorporating the imposed boundary conditions given by Eq. A-11:

$$\int_0^S K_2\, dx = \int_0^S u_x\, dx$$

or

$$K_2 = 1 - \frac{L}{S} \qquad \text{(A-25)}$$

Reproduced with permission of the copyright owner. Further reproduction prohibited without permission.

Substituting Eq. A-23 into Eq. A-19 and performing the indicated integration, the element strain energy for the tension member in the inelastic range is given by:

$$U = AS\left[\tfrac{1}{2}E\varepsilon_e^2 + f\varepsilon_e + \frac{1}{24g}(-8g\varepsilon_e + 4f^2 - 4c)^{3/2}\right]$$

$$+ AS\, f(K_2 + \tfrac{1}{2}K_2^2 + \varepsilon_p) - \frac{AS}{24g}\left[-8g(K_2 + \tfrac{1}{2}K_2^2 + \varepsilon_p)\right.$$

$$\left. + 4f^2 - 4c\right]^{3/2} \qquad \text{(A-26)}$$

III. <u>Elastic Analysis of Compression Members</u>

A general truss element in the undeformed and deformed states is shown in Fig. 3. The initial undeformed length (L) is given by Eq. A-1, and the deformed length (S) is given by Eq. A-2.

The strain-deformation relation is given by

$$\varepsilon = u_x + \tfrac{1}{2}w_x^2 - zw_{xx} \qquad \text{(A-27)}$$

where z is measured from the neutral axis of the cross-section in the plane of bending.

Integration of the strain energy density definition

$$dU = \int_0^{\varepsilon+\varepsilon_p} \sigma \, d\varepsilon$$

Reproduced with permission of the copyright owner. Further reproduction prohibited without permission.

under the assumption of ideal linear elastic material behaviour,

$$\sigma = E(\varepsilon + \varepsilon_p)$$

gives the element strain energy as

$$U = \frac{E}{2} \int_V (\varepsilon + \varepsilon_p)^2 \, dV$$

Substitution for the strain from Eq. A-27 and integrating over the cross section yields the strain energy in terms of the local deformations (u,w) of the element:

$$U = \frac{E}{2} \int_0^S \int_A (u_x + \tfrac{1}{2}w_x^2 - zw_{xx} + \varepsilon_p)^2 \, dA \, dX$$

$$= \frac{E}{2} \int_0^S \int_A \Big\{ (u_x + \tfrac{1}{2}w_x^2 + \varepsilon_p)^2 - 2z(u_x + \tfrac{1}{2}w_x^2 + \varepsilon_p)$$

$$+ z^2 w_{xx}^2 \Big\} \, dA \, dx$$

Since, $\int_A dA = A$, $\int z \, dA = 0$ and

$\int_A z^2 \, dA = I$ (section's moment of inertia)

Reproduced with permission of the copyright owner. Further reproduction prohibited without permission.

therefore,

$$U = \frac{AE}{2} \int_0^S \left\{ (u_x + \tfrac{1}{2}w_x^2 + \varepsilon_p)^2 + \frac{I}{A} w_{xx}^2 \right\} dx \qquad \text{(A-28)}$$

Taking the first variation of Eq. A-28, integrating by parts and rearranging terms gives:

$$\delta U = 0 = -AE \int_0^S \left\{ \frac{d}{dx} (u_x + \tfrac{1}{2}w_x^2 + \varepsilon_p) \right\} \delta u \, dx \qquad \text{(a)}$$

$$+AE \int_0^S \left\{ \frac{I}{A} w_{xxxx} - \frac{d}{dx} \left[(u_x + \tfrac{1}{2}w_x^2 + \varepsilon_p) \, w_x \right] \right\} \delta w \, dx \qquad \text{(b)}$$

$$+AE \left| (u_x + \tfrac{1}{2}w_x^2 + \varepsilon_p) \, \delta u \right|_0^S \qquad \text{(c)}$$

(A-29)

$$-AE \left| \left\{ \frac{I}{A} w_{xxx} - (u_x + \tfrac{1}{2}w_x^2 + \varepsilon_p) w_x \right\} \delta w \right|_0^S \qquad \text{(d)}$$

$$+EI \left| (w_{xx}) \, \delta w_x \right|_0^S \qquad \text{(e)}$$

Each of the contributions (a) through (e) in Eq. A-29 must individually be zero, and since the variations δu and δw are arbitrary:

Reproduced with permission of the copyright owner. Further reproduction prohibited without permission.

$$\frac{d}{dx}\left(u_x + \tfrac{1}{2}w_x^2 + \epsilon_p\right) = 0 \tag{A-30}$$

and

$$\frac{I}{A}\, w_{xxxx} - \frac{d}{dx}\left[\left(u_x + \tfrac{1}{2}w_x^2 + \epsilon_p\right)w_x\right] = 0 \tag{A-31}$$

Equations A-30 and A-31 represent the governing differential equations for the general truss discrete element. Integrating Eq. A-30 gives

$$u_x + \tfrac{1}{2}w_x^2 + \epsilon_p = K_3 \tag{A-32}$$

Since K_3 is constant with respect to x, Eq. A-31 can be written in the form

$$w_{xxxx} - \frac{AK_3}{I}\, w_{xx} = 0 \tag{A-33}$$

The rotations of the ends of the general truss element are not imposed since moment free joints have been assumed; therefore, the variational quantity δw_x in contribution (e) of Eq. A-29 is arbitrary at the ends of the element and the term in braces must be zero. The natural boundary conditions are then:

$$w_{xx}\Big|_{x=0} = 0\ ,\quad w_{xx}\Big|_{x=S} = 0 \tag{A-34}$$

Reproduced with permission of the copyright owner. Further reproduction prohibited without permission.

The variational quantities δu and δw in contributions (c) and (d) of Eq. A-29 are prescribed zero on the boundaries. From Fig. 3, the imposed boundary conditions are

$$u\Big|_{x=0} = 0 \;,\; u\Big|_{x=S} = S - L \tag{A-35}$$

and

$$w\Big|_{x=0} = 0 \;,\; w\Big|_{x=S} = 0 \tag{A-36}$$

As the variational quantity δu vanishes at the ends of the element, Eq. A-29(c) and Eq. A-32 indicate that the force in the general truss element is a constant given by

$$F = AEK_3 \tag{A-37}$$

The general solution of Eq. A-33 is given by

$$w = B_1 + B_2 x + B_3 \sin\sqrt{\frac{-AK_3}{I}}\,x + B_4 \cos\sqrt{\frac{-AK_3}{I}}\,x \tag{A-38}$$

where $K_3 < 0$ for compression members (Eq. A-27), which are capable of having nonzero values of the deformation w when buckling occurs. The natural boundary conditions given by Eq. A-34, together with the imposed boundary conditions given by Eq. A-36 are substituted in Eq. A-38 to solve for the four constants, which results in

Reproduced with permission of the copyright owner. Further reproduction prohibited without permission.

$$B_1 = B_2 = B_3 = 0$$

$$B_3 \sin \sqrt{\frac{-AK_3}{I}}\, S = 0$$

If the trivial solution is disregarded, then K_3 must be treated as an eigenvalue

$$K_{3cr} = -\left(\frac{m\pi}{S}\right)^2 \frac{I}{A}, \quad m=1,2,... \qquad \text{(A-39)}$$

According to Eq. A-37; the critical force (buckling load) in the member is given by:

$$F_{cr} = -\left(\frac{m\pi}{S}\right)^2 EI, \quad m=1,2,... \qquad \text{(A-40)}$$

Substituting Eq. A-39 into Eq. A-38, the eigenvalues corresponding to the critical values of K_3 are obtained as

$$w_m = B_m \sin \frac{m\pi x}{S}, \quad m=1,2,... \qquad \text{(A-41)}$$

The assumed local transverse deformation mode of a general truss member is taken to be proportional to the first buckling eigenmode

Reproduced with permission of the copyright owner. Further reproduction prohibited without permission.

$$w = C \sin \frac{\pi x}{S} \qquad \text{(A-42)}$$

The constant C defining the midspan displacement is retained in the formulation as a generalized coordinate.

The constant K_3 now can be determined by integrating Eq. A-32 over the length

$$\int_0^S K_3 dx = \int_0^S (u_x + \tfrac{1}{2} w_x^2 + \varepsilon_p)\, dx$$

or

$$K_3 = 1 - \frac{L}{S} + \varepsilon_p + \left(\frac{\pi C}{2S}\right)^2 \qquad \text{(A-43)}$$

The element strain energy is obtained in terms of the nodal displacements and the buckling amplitude upon substituting Equations A-32, A-43 and A-42 into Eq. A-28 and performing the indicated integration:

$$U = \frac{AE}{2}\left[SK_3^2 + \tfrac{1}{2}\, \frac{I}{A}\, \frac{\pi^4 C^2}{S^3} \right] \qquad \text{(A-44)}$$

IV. Element Stiffness Second Partials Matrix

The scaling transformation technique recommended to improve the convergence of the Fletcher-Reeves algorithm to the minimum of the total potential energy of the structure (Chapter III), requires the evaluation

Reproduced with permission of the copyright owner. Further reproduction prohibited without permission.

of the diagonal matrix [R] with diagonal elements

$$r_{jj} = \frac{1}{(k_{jj})^{\frac{1}{2}}}\ , \quad j = 1,2,\ldots,N \tag{A-45}$$

where [K] = (k_{jj}) is the matrix of second partials of the quadratic terms in the total potential energy, and N is the total number of displacement degrees of freedom. The elements of the matrix [K] are computed from the element stiffness second partials matrices by the use of a variable correlation scheme. The diagonal elements of the matrix of second partial derivatives of the element stiffness matrix are obtained by partially differentiating the expressions of Eq. 2.30 with respect to each of the element seven degrees of freedom, as follows

$$\frac{\partial^2 U}{\partial \tilde{u}_p^2} = -\frac{AE}{2}\left[-f_3 + \left[(\tilde{X}_q + \tilde{u}_q) - (\tilde{X}_p + \tilde{u}_p)\right]\frac{\partial f_3}{\partial \tilde{u}_p}\right]$$

$$\frac{\partial^2 U}{\partial \tilde{v}_p^2} = -\frac{AE}{2}\left[-f_3 + \left[(\tilde{Y}_q + \tilde{v}_q) - (\tilde{Y}_p + \tilde{v}_p)\right]\frac{\partial f_3}{\partial \tilde{v}_p}\right]$$

$$\frac{\partial^2 U}{\partial \tilde{w}_p^2} = -\frac{AE}{2}\left[-f_3 + \left[(\tilde{Z}_q + \tilde{w}_q) - (\tilde{Z}_p + \tilde{w}_p)\right]\frac{\partial f_3}{\partial \tilde{w}_p}\right]$$

Reproduced with permission of the copyright owner. Further reproduction prohibited without permission.

$$\frac{\partial^2 U}{\partial \tilde{u}_q^2} = \frac{\partial^2 U}{\partial \tilde{u}_p^2}$$

$$\frac{\partial^2 U}{\partial \tilde{v}_q^2} = \frac{\partial^2 U}{\partial \tilde{v}_p^2}$$

$$\frac{\partial^2 U}{\partial \tilde{w}_q^2} = \frac{\partial^2 U}{\partial \tilde{w}_p^2}$$

$$\frac{\partial^2 U}{\partial c^2} = \frac{AE}{2} \left[\frac{\pi^2 K_3}{S} + \frac{\pi^4 C^2}{2S^3} + \frac{I}{A} \frac{\pi^4}{S^3} \right]$$

where f_3 is given by

$$f_3 = \frac{K_3^2}{S} + 2K_3 \frac{L}{S^2} - \frac{\pi^2 C^2}{S^3} K_3 - \frac{3}{2} \frac{I}{A} \frac{\pi^4 C^2}{S^5}$$

Experience has proven that considering the linear terms only in the above expressions is sufficient to form the required scaling transformation matrix. This is obtained by considering the approximations

$$L = S \text{ and } C = 0$$

Reproduced with permission of the copyright owner. Further reproduction prohibited without permission.

This leads to the following expressions:

$$K_{11} = -\frac{AE}{2}\left[f_4 + \frac{1}{L^3}(\tilde{X}_q - \tilde{X}_p)^2\left[-2(1+\varepsilon_p)^2 + 3f_4L\right]\right]$$

$$K_{22} = -\frac{AE}{2}\left[f_4 + \frac{1}{L^3}(\tilde{Y}_q - \tilde{Y}_p)^2\left[-2(1+\varepsilon_p)^2 + 3f_4L\right]\right]$$

$$K_{33} = -\frac{AE}{2}\left[f_4 + \frac{1}{L^3}(\tilde{Z}_q - \tilde{Z}_p)\left[-2(1+\varepsilon_p)^2 + 3f_4L\right]\right]$$

$$K_{44} = K_{11}$$

$$K_{55} = K_{22} \qquad \text{(A-47)}$$

$$K_{66} = K_{33}$$

$$K_{77} = \frac{AE}{2}\left[\frac{\pi^2\varepsilon_p}{L} + \frac{I}{A}\frac{\pi^4}{L^3}\right]$$

where f_4 is given by

$$f_4 = \frac{\varepsilon_p^2}{L} + \frac{2\varepsilon_p}{L}$$

Reproduced with permission of the copyright owner. Further reproduction prohibited without permission.

APPENDIX B

DETERMINATION OF THE INITIAL SHAPE OF A SUSPENSION STRUCTURE

In prestressed suspension structures the initial shape of the structure is dependent upon the prestress forces and must satisfy the equilibrium conditions. In general, the initial position of a suspension structure can easily be determined by considering the equilibrium at the structure's joints.

Consider the equilibrium of a general joint (a) of a general non-orthogonal cable net as shown in Fig. B-1. The horizontal components in the cables extending in the m-direction must be equal to each other in order to satisfy equilibrium in that direction. This horizontal component is denoted by H_m. Similarly, the horizontal components in the cables extending in the n-direction must be equal and is denoted by H_n.

The vertical components of the tensions in the cables segments meeting at joint (a) shall satisfy the vertical equilibrium:

$$V_{ab} + V_{ac} + V_{ad} + V_{ae} = 0 \qquad \text{(B-1)}$$

Reproduced with permission of the copyright owner. Further reproduction prohibited without permission.

where the vertical components are given by the relations:

$$V_{ab} = H_m \left[\frac{Z_b - Z_a}{\ell_{ab}} \right]$$

$$V_{ac} = H_m \left[\frac{Z_c - Z_a}{\ell_{ac}} \right]$$

$$V_{ad} = H_n \left[\frac{Z_d - Z_a}{\ell_{ad}} \right] \qquad \text{(B-2)}$$

$$V_{ae} = H_n \left[\frac{Z_e - Z_a}{\ell_{ae}} \right]$$

where ℓ is the length of a cable segment in the horizontal X-Y plane and Z_a, Z_b, Z_c, Z_d, Z_e are the vertical coordinates to be determined.

Substituting Eq. B-2 into Eq. B-1 gives:

$$H_m \left[\frac{Z_b - Z_a}{\ell_{ab}} + \frac{Z_c - Z_a}{\ell_{ac}} \right] + H_n \left[\frac{Z_d - Z_a}{\ell_{ad}} + \frac{Z_e - Z_a}{\ell_{ae}} \right] = 0 \qquad \text{(B-3)}$$

For given values of H_m, H_n, and the coordinates of the joints on the boundary of the net, Eq. B-3 leads to a system of p simultaneous linear algebraic equations for

Reproduced with permission of the copyright owner. Further reproduction prohibited without permission.

the p unknown values of z-coordinates. These equations can easily be expressed in a matrix form as follows:

The p joints of the net where the Z coordinates are unknown are assigned numbers from 1 to p, and the q joints where the Z coordinates are known are assigned numbers from p+1 to r, where r ($r=p+q$) is equal to the total number of the net joints.

Define a vector {Z} given by:

$$\{Z\} = \left\{\begin{array}{c} Z_1 \\ Z_2 \\ \vdots \\ Z_p \\ -- \\ Z_{p+1} \\ \vdots \\ Z_r \end{array}\right\} \qquad \text{(B-4)}$$

The equilibrium of the forces at each joint (Eq. B-3) can then be written in a matrix form as

$$\underset{(p\times r)}{[H]} \quad \underset{(r\times 1)}{\{Z\}} = \underset{(p\times 1)}{\{O\}} \qquad \text{(B-5)}$$

Reproduced with permission of the copyright owner. Further reproduction prohibited without permission.

Eq. B-5 can be partitioned in the form

$$\begin{bmatrix} \underset{(p\times p)}{H_p} & \vdots & \underset{(p\times q)}{H_q} \end{bmatrix} \cdot \begin{Bmatrix} \underset{(p\times 1)}{Z_p} \\ \hline \underset{(q\times 1)}{Z_q} \end{Bmatrix} = \begin{Bmatrix} 0 \\ \hline 0 \end{Bmatrix} \qquad \text{(B-6)}$$

The vector $\{Z_p\}$ contains the p unknown Z coordinates of joints, and the vector $\{Z_q\}$ contains the q known Z coordinates of joints. Eq. B-6 can be rewritten as:

$$\underset{(p\times p)}{[H_p]}\ \underset{(p\times 1)}{\{Z_p\}} + \underset{(p\times q)}{[H_q]}\ \underset{(q\times 1)}{\{Z_q\}} = \underset{p\times 1}{\{0\}} \qquad \text{(B-7)}$$

and the solution for $\{Z_p\}$ is given by

$$\{Z_p\} = -[H_p]^{-1}[H_q]\{Z_q\} \qquad \text{(B-8)}$$

The inverse of the matrix $[H_p]$ can be obtained by using the direct method of Gauss Elimination, and the solution for $\{Z_p\}$ is obtained directly by performing the matrix multiplication in Eq. B-8.

Reproduced with permission of the copyright owner. Further reproduction prohibited without permission.

APPENDIX C

EQUILIBRIUM EQUATIONS OF PRESTRESS FORCES IN THE UNLOADED CABLE NET OF EXAMPLE L2

The suspended roof of example L2 was analyzed analytically and experimentally by Siev in Ref. 2.

The equilibrium in the horizontal plane $(\tilde{X},\tilde{Y})$ of the horizontal prestress components forces in the unloaded system gives the relation between the horizontal component (H) of prestress in all diagonal cables, and (H_1) of the main cables (Fig. C-1):

In the $\tilde{X}$-direction:

$$H + H_1 \cos\theta = H_1 \cos 45^\circ \tag{C-1}$$

In the $\tilde{Y}$-direction:

$$H + H_1 \sin 45^\circ = H_1 \cos\theta \tag{C-2}$$

From the previous two equations:

$$\frac{H_1 \sin 45^\circ + H}{H_1 \cos 45^\circ - H} = \tan\theta \tag{C-3}$$

Reproduced with permission of the copyright owner. Further reproduction prohibited without permission.

From the geometry of Fig. C1 (geometry of model studied by Siev experimentally):

$$\tan\theta = \frac{a/2 + \delta\sqrt{2}}{a/2} \qquad \text{(C-4)}$$

Substituting Eq. C-4 in Eq. C-3 gives

$$H_1 = \frac{\sqrt{2}}{\delta}\left[\frac{a}{\sqrt{2}} + \delta\right] H \qquad \text{(C-5)}$$

The numerical values of a and δ are given by Siev as:

$$a = 60.6090 \text{ and } \delta = 14.2857$$

Thus the relation between H and H_1 is given by

$$H_1 = 5.65684\ H$$

In Fig. C-1, points 3,4,7 and 8 are at mid-height ($\tilde{Z} = 0.0$); where 1 and 2 are symmetrical with respect to mid-height. In other words, an equilibrium equation of the vertical prestress components forces in the unloaded system contains a single unknown - the elevation $\pm f$ of points 0,1,2,5,6,9,10, and 11 - where the height is equal to 63.5 cms:

$$\frac{H}{2} f + \frac{2H}{a\sqrt{2}} f - \frac{H_1}{a\sqrt{2} + \delta}\left[\frac{63.5}{2} - f\right] = 0 \qquad \text{(C-6)}$$

Reproduced with permission of the copyright owner. Further reproduction prohibited without permission.

On substituting H_1 from Eq. C-5 into Eq. C-6, H is eliminated. Rearranging and simplifying gives

$$f = \frac{63.5}{\sqrt{2}} \frac{a}{3\delta + 2\sqrt{2}\, a}$$

or

$$f = 12.7 \text{ cm}$$

Thus the elevations of all the cable net nodes are determined (Fig. 5).

Reproduced with permission of the copyright owner. Further reproduction prohibited without permission.

VITA AUCTORIS

1949 Born on January 1st in Fayoum, Egypt.

1971 Graduated with a B.Sc.(honrs.) in Civil Engineering from Cairo University.

1971 Joined the Suez Canal Authority, Egypt, as a Structural Engineer.

1973 In September, 1973, enrolled at the University of Windsor in a programme leading to the degree of Master of Applied Science in Civil Engineering.

Reproduced with permission of the copyright owner. Further reproduction prohibited without permission.